

Atomistic simulations of molten carbonates: thermodynamic and transport properties of the $\text{Li}_2\text{CO}_3\text{-Na}_2\text{CO}_3\text{-K}_2\text{CO}_3$ system

Elsa Desmaele,^{1, a)} Nicolas Sator,¹ Rodolphe Vuilleumier,² and Bertrand Guillot^{1, b)}

¹⁾*Sorbonne Université, CNRS, Laboratoire de Physique*

Théorique de la Matière Condensée, LPTMC, F75005, Paris,

France

²⁾*PASTEUR, Département de chimie, École normale supérieure,*

PSL University, Sorbonne Université, CNRS, 75005 Paris,

France

(Dated: 7 February 2019)

Although molten carbonates only represent, at most, a very minor phase in the Earth's mantle, they are thought to be implied in anomalous high-conductivity zones in its upper part (70–350 km). Besides the high electrical conductivity of these molten salts is also exploitable in fuel cells. Here we report quantitative calculations of their properties, over a large range of thermodynamic conditions and chemical compositions, that are a requisite to develop technological devices and to provide a better understanding of a number of geochemical processes.

To model molten carbonates by atomistic simulations, we have developed an optimized classical force field based on experimental data of the literature and on the liquid structure issued from ab initio molecular dynamics simulations performed by ourselves. In implementing this force field into a molecular dynamics simulation code, we have evaluated the thermodynamics (equation of state and surface tension), the microscopic liquid structure and the transport properties (diffusion coefficients, electrical conductivity and viscosity) of molten alkali carbonates (Li_2CO_3 , Na_2CO_3 , K_2CO_3 and some of their binary and ternary mixtures) from the melting point up to the thermodynamic conditions prevailing in the Earth's upper mantle (~ 1100 – 2100 K, 0–15 GPa). Our results are in very good agreement with the data available in the literature. To our knowledge a reliable molecular model for molten alkali carbonates covering such a large domain of thermodynamic conditions, chemical compositions and physicochemical properties has never been published yet.

Keywords: molten carbonates, molecular dynamics simulations, equation of state, microscopic structure, transport properties, surface tension

^{a)}Electronic mail: elsa.desmaele@gmail.com

^{b)}Electronic mail: guillot@lptmc.jussieu.fr

I. INTRODUCTION

Carbonate melts receive an increasing interest in both fundamental and applied fields either in the view of developing technological devices (e.g. fuel cell technology)¹⁻⁵ or for providing a better understanding of a number of geochemical processes (e.g. role of molten carbonates in the geodynamics of the Earth's mantle).⁶⁻⁹ The study of the physicochemical properties (thermodynamics, structure and transport) of, mainly alkali, molten carbonates, under atmospheric pressure has been initiated by the electrochemistry community a few decades ago.¹⁰ These systems were depicted as highly conducting liquids of low viscosity. From a geosciences viewpoint the focus is more recent and mainly set on alkaline-earth compositions under high pressures, whose properties are so far poorly known.^{6,11,12} Indeed studies of these liquids at high $T - P$ require very specific devices adapted to the measurement a single observable. On the contrary, in a molecular dynamics simulation a number of properties can be obtained at once, even at extreme thermodynamic conditions. However molecular dynamics simulations require the knowledge of atomic interactions in the system under consideration. These interactions (the force field) can be deduced from electronic structure calculations (*ab initio*) or based on a more empirical approach (classical molecular dynamics or simply referred to as MD in the following). The former method, although *a priori* more accurate than the latter one is computationally much more demanding (by several orders of magnitude) and is thus inappropriate when the aim of the study is to span a large range of chemical composition and thermodynamic conditions. On the other hand, the relevance of a MD calculation relies on the quality of the implemented force field (FF) whose adjustment is system-specific. Since the first attempts by Janssen and Tissen¹³⁻¹⁵ to model molten carbonates by two-body interactions, several modifications have been suggested.¹⁶⁻²⁰ However the FF of Janssen and Tissen¹³ has some inherent defects. For instance the calculated pressure is shifted by ~ 15 kbar,¹⁹ at the 1-bar experimental density. A decisive improvement towards an accurate description of the properties of molten carbonates in quantitative agreement with the experiments came with the force fields (FF) of Vuilleumier *et al.*²¹ and Corradini *et al.*²² However these models are restricted in composition, to pure CaCO_3 and to the Li_2CO_3 - K_2CO_3 (62:38 mol%) eutectic mixture respectively. For the sake of conciseness and clarity of the comparisons with the experimental literature, alkaline-earth compositions will be investigated in a companion paper.²³ Here we present MD

simulation results that sketch a systematic and consistent model of molten carbonates in the $\text{Li}_2\text{CO}_3\text{-Na}_2\text{CO}_3\text{-K}_2\text{CO}_3$ system over a large $T - P$ range ($\sim 1100\text{-}2100$ K, $0\text{-}15$ GPa). After presenting the details of the simulations, we discuss the thermodynamic properties (equation of state and surface tension), the liquid structure and the transport properties (diffusion coefficients, electrical conductivity and viscosity).

II. COMPUTATIONAL DETAILS

A. Ab initio molecular dynamics (AIMD)

The *ab initio* molecular dynamics (AIMD) simulations were based on the density functional theory (DFT) within the Born-Oppenheimer framework. They were performed thanks to the free QUICKSTEP/CP2K software²⁴ that applies a hybrid Gaussian plane-wave method.²⁵ For valence electrons, we used a double-zeta valence plus polarization (DZVP) basis set optimized for molecules,²⁶ while core electrons were replaced by the Goedecker-Teter-Hutter (GTH) norm-conserving pseudo-potentials.²⁷⁻²⁹ The cutoff for the electronic density was set to 700 Ry. Exchange and correlation interactions were accounted for by the gradient corrected BLYP functional^{30,31} using a semi-empirical D3 dispersion correction scheme with a 30 Å cutoff.³² All DFT calculations were run in the NVT ensemble with the temperature set constant by a Nosé-Hoover thermostat.^{33,34} Timestep was fixed to 0.5 fs, and simulation run was of the order of 13–48 ps.

The starting configurations were issued from classical MD runs using a guess force field. Na_2CO_3 and K_2CO_3 simulations were performed at state points corresponding to their atmospheric melting point,^{35,36} that is respectively (1140 K, 1.97 g/cm^3) and (1190 K, 1.90 g/cm^3), where densities were set to their experimental values.³⁷ The pressure calculated along both runs is 0 ± 0.5 GPa, as expected. To investigate the high pressure behavior, a third simulation was performed for K_2CO_3 at 1773 K and 2.41 g/cm^3 leading to a calculated pressure of 6 ± 1.5 GPa. Table S1 summarizes the simulation details of the three AIMD simulations. Note that the AIMD simulation of Corradini *et al.*²² for the $\text{Li}_2\text{CO}_3\text{-K}_2\text{CO}_3$ eutectic mixture uses similar methodological features, and hence it will be considered as a benchmark for Li-bearing compositions investigated here by MD.

B. Classical molecular dynamics (MD)

Classical MD simulations were carried out using the free DL_Poly_2 software.³⁸ The timestep was set to 1 fs and the studied systems were composed of $N \simeq 2000$ atoms. To evaluate the equation of state (EoS) as discussed in section IV A, calculations in the NPT ensemble were performed. The total simulation time was 0.9 ns, including a 0.5 ns equilibration with a Nosé-Hoover thermostat, to reach a statistical accuracy on the density of about $\Delta n/n \leq \pm 1\%$. For transport coefficients, production runs of 10 to 30 ns were performed in the NVE ensemble. Structure data were extracted from the same simulations. Note that for a better comparison with the AIMD-generated pair distribution functions (see section III), some MD simulations were also specifically run on systems having the same density and number of atoms.

III. FORCE FIELD

i	j	A_{ij} (kJ/mol)	ρ_{ij} (Å)	C_{ij} (Å ⁶ /mol)	q_i (e)
Li	O	3.0×10^5	0.2228	1210	+0.82101
Na	O	11×10^5	0.2228	3000	+0.82101
K	O	9.0×10^5	0.2570	7000	+0.82101
O	O	5.0×10^5	0.252525	2300	-0.89429
C	O	0	1	0	+1.04085

TABLE I. Intermolecular potential parameters and partial charges. Note that the Born repulsion parameters between oxygen atoms of a same carbonate ion are $A_{OO}^{intra-CO_3} = 2611707.2$ kJ/mol and $\rho_{OO}^{intra-CO_3} = 0.22$ Å.

The empirical force field is derived from an interaction potential summing the pair interactions between the atoms of a same carbonate molecule (intramolecular potentials V_{ij}^{intra}) and those between atom pairs belonging to different ions (intermolecular potentials V_{ij}^{inter}). The carbonate molecule is featured as flexible and non-dissociative by introducing the following pair potential between C and O atoms:

$$V_{CO}^{intra-CO_3}(r_{CO}) = \frac{1}{2}k_{CO}(r_{CO} - r_{0,CO})^2 + q_O q_C / 4\pi\epsilon_0 r_{CO} \quad . \quad (1)$$

The force constant $k_{\text{CO}} = 6118.17$ kJ/mol and the harmonic equilibrium distance $r_{0,\text{CO}} = 1.30$ Å are adjusted so as to obtain a mean C-O distance of 1.29 Å.^{21,39} Moreover the coulombic interactions are implemented in order to prevent the atomization of the molecule at high pressure. The oxygen atoms of a same molecule repel one another via the pair potential:

$$V_{\text{OO}}^{\text{intra-CO}_3}(r_{\text{OO}}) = A_{\text{OO}}^{\text{intra-CO}_3} \exp(-r_{\text{OO}}/\rho_{\text{OO}}^{\text{intra-CO}_3}) . \quad (2)$$

The latter one ensures on average the planarity of the carbonate ion, where $A_{\text{OO}}^{\text{intra-CO}_3} = 2611707.2$ kJ/mol and $\rho_{\text{OO}}^{\text{intra-CO}_3} = 0.22$ Å. The intermolecular interactions are ruled by the pair potential:

$$V_{ij}^{\text{inter}}(r_{ij}) = A_{ij} \exp(-r_{ij}/\rho_{ij}) - C_{ij}/r_{ij}^6 + q_i q_j / 4\pi\epsilon_0 r_{ij} , \quad (3)$$

with $i, j = \text{O, C, Li, Na, K}$. The van der Waals part (first two terms) of this potential is set to zero between cations, thus enabling a straightforward transferability of the force field to any carbonate mixture in the Li–Na–K system. Parameters of the FF are summarized in Table I. While the charges were constrained by the FF of Vuilleumier *et al.*²¹, the van der Waals interactions have been benchmarked on experimental volumetric studies and on AIMD structure data (note that dispersion interactions have little effect on the shape of the pair distribution functions, but affects strongly the density). Thus atmospheric density and compressibility³⁷ are accurately reproduced by our model as discussed in section IV. The suitability of the force field was further constrained by fitting at best the pair distribution functions of AIMD simulations, obtained either by Corradini *et al.*²² for the Li_2CO_3 – K_2CO_3 eutectic mixture of ratio 0.62:0.38 mol% (LKe), or specifically calculated by ourselves for Na_2CO_3 and K_2CO_3 . The agreement between MD simulations and AIMD structure data is excellent (Figure S1). Notice that for LKe in particular, the fitting of the AIMD curves by MD is at least as good, as when using Corradini *et al.*'s FF (Figure 1 of reference 22). The microscopic structure is thoroughly described in section IV B.

To be complete, and although the present FF is not aimed at studying the crystalline phase, we checked its ability to reproduce the experimentally determined structures of the monoclinic crystals of Li_2CO_3 , Na_2CO_3 and K_2CO_3 at room conditions. The densities calculated by anisotropic relaxation (*NST* ensemble) of these structures are 2.12 g/cm³ for Li_2CO_3 , 2.50 g/cm³ for Na_2CO_3 and 2.45 g/cm³ for K_2CO_3 to be compared to 2.10, 2.54 and 2.44 g/cm³, respectively^{40–42} (see also Table S2 for lattice parameters).

	n_{1100K} (g/cm ³)		α (10 ⁻⁴ g/cm ³ /K)	
	MD	Exp	MD	Exp
Li ₂ CO ₃	1.796	1.792 \blacklozenge	4.251	3.729 \blacklozenge
		1.793 \blacktriangle		3.385 \blacktriangle
		1.795 \blackstar		3.459 \blackstar
Na ₂ CO ₃	1.991	1.986 \blacklozenge	5.515	4.487 \blacklozenge
		1.980 \blacktriangle		4.696 \blacktriangle
		1.988 \blackstar		4.511 \blackstar
K ₂ CO ₃	1.931	1.928 \blacklozenge	4.222	4.421 \blacklozenge
		1.925 \blacktriangle		3.563 \blacktriangle
		1.939 \blackstar		4.615 \blackstar

TABLE II. Density and thermal expansion coefficient ($n = n_{1100K} - \alpha(T - 1100)$) from MD simulations and comparison with the experimental literature: references 10 (\blacklozenge), 43 (\blacktriangle) and 37 (\blackstar).

	T_{ref} (K)	n_{ref}^0 (g/cm ³)	α_0 (K ⁻¹)	α_1 (K ⁻²)	K_{ref}^0 (GPa)	b_1 (K ⁻¹)	b_2 (K ⁻²)	K'^0	T (K)	P (GPa)
Li ₂ CO ₃	1100	1.80	-2.57 $\times 10^{-4}$	2.41 $\times 10^{-8}$	12.56	9.4 $\times 10^{-4}$	8.5 $\times 10^{-7}$	8.0	1100-1923	0-6
Na ₂ CO ₃	1140	1.97	-2.64 $\times 10^{-4}$	-4.61 $\times 10^{-8}$	9.01	11.4 $\times 10^{-4}$	12.7 $\times 10^{-7}$	8.5	1100-2073	0-15
K ₂ CO ₃	1190	1.89	-2.56 $\times 10^{-4}$	-10.05 $\times 10^{-8}$	5.96	12.0 $\times 10^{-4}$	12.2 $\times 10^{-7}$	7.6	1100-2073	0-15

TABLE III. Parameters of the third-order Birch Murnaghan equation of state and $T - P$ domain of validity for each pure end-member composition. See text and equations (4), (5) and (6) for details.

IV. THERMODYNAMICS

A. Equation of state

The density of molten alkali carbonates at atmospheric pressure has been reported by several experimental studies.^{10,37,43–48} For the pure end-members, Li₂CO₃, Na₂CO₃ and K₂CO₃ a global consistency between these studies is found. Using the present FF, MD fits very well the above studies considering the small experimental uncertainties and the very limited temperature range (~ 100 K) investigated at 1 bar (Table II). In this context notice that the model of Corradini *et al.*²² recovers reasonably the 1-bar density of K₂CO₃, but it doesn't perform as well for pure Li₂CO₃, the deviations reaching -5 %.

	LKe	LNKe
n_{Exp}^0 (g/cm ³)	1.88	1.91
n_{MD}^0 (g/cm ³)	1.88 (1.85 [†])	1.91
$n_{MD,mix}^0$ (g/cm ³)	1.87	1.91
K_{Exp}^0 (GPa)	8.9	9.1
K_{MD}^0 (GPa)	8.6 (6.81 [†])	8.9
$K_{MD,mix}^0$ (GPa)	8.6	8.8

TABLE IV. Density and bulk modulus of the LKe and LNKe mixtures at $T = 1100$ K calculated either by MD simulation (n_{MD}^0 , K_{MD}^0) or by using ideal mixing rules ($n_{MD,mix}^0$, $K_{MD,mix}^0$). Experimental data n_{Exp}^0 , K_{Exp}^0 are given for comparison.³⁷ Results issued from the MD model of Corradini *et al.*²² ([†]) are given in parenthesis.

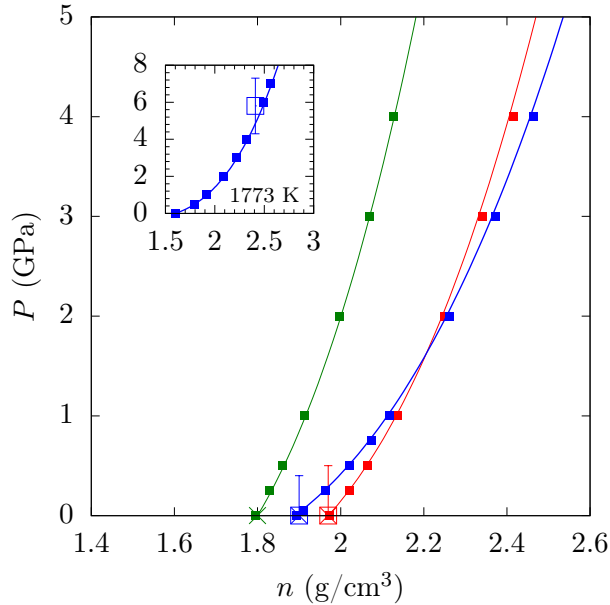


FIG. 1. Compression isotherms of molten Li_2CO_3 (green), Na_2CO_3 (red) and K_2CO_3 (blue) at their respective melting temperature: plain squares are MD simulations, open squares are AIMD simulations and crosses are experimental data of Liu and Lange.³⁷ The isotherms (full curves) were obtained by interpolating the MD points with the third-order Birch-Murnaghan equation (see text). In the inset are shown the 1773 K MD isotherm for K_2CO_3 and the AIMD result at the same temperature and 2.41 g/cm³.

Despite the geochemical interest for assessing the buoyancy of carbonated fluids in the mantle, no systematic measurements of liquid density at high pressure have been reported yet, except for the study of Dobson *et al.*,⁴⁹ for K_2CO_3 at 4 GPa. Besides the study of Dobson *et al.* has since been challenged by Liu *et al.*⁵⁰ These latter authors provided estimates of high pressure volumetric behavior for K_2CO_3 ,^{37,50} by using the third-order Birch Murnaghan equation of state (BMEoS)⁵¹ that is well-known for its accuracy in the modeling of the compressibility of molten and crystalline silicates.^{52,53} It writes:

$$P = \frac{3}{2}K^0(T) \left(\left(\frac{n}{n_T^0} \right)^{7/3} - \left(\frac{n}{n_T^0} \right)^{5/3} \right) \times \left(1 - \frac{3}{4}(4 - K'^0) \left(\left(\frac{n}{n_T^0} \right)^{2/3} - 1 \right) \right), \quad (4)$$

where n_T^0 is the atmospheric density at temperature T , K_T^0 the bulk modulus and K'^0 its pressure derivative at 1 bar. Such an equation expressing the density of the carbonated liquid at any thermodynamic condition is appealing, although K'^0 has so far only been derived by indirect thermodynamic considerations (see below).

To determine the BMEoS of liquid Li_2CO_3 , Na_2CO_3 and K_2CO_3 from MD, their density was calculated along several isotherms at different pressures. The values of n_T^0 and $K^0(T)$ were fitted by using empirical temperature dependencies:

$$n_T^0 = n_{ref}^0 e^{\int_{T_{ref}}^T -(\alpha_0 + \alpha_1 T) dT}, \quad (5)$$

and

$$K_T^0 = \frac{K_{ref}^0}{1 + b_1(T - T_{ref}) + b_2(T - T_{ref})^2}. \quad (6)$$

The reference temperature T_{ref} is defined for numerical purposes and set to the atmospheric melting point for each composition (Table III), n_{ref}^0 and K_{ref}^0 are the density and bulk modulus at 1-bar and T_{ref} . Values of the parameters α_0 , α_1 , b_1 and b_2 are given in Table III.

The excellent agreement between calculated points and the fitted isotherms (Figures 1 and S2) illustrates the ability of the BMEoS to describe carbonate melts, at least on the investigated pressure-temperature range. Furthermore, the obtained BMEoS for Li_2CO_3 , Na_2CO_3 and K_2CO_3 match not only the experimental values at 1 bar, but also those of our AIMD calculations. However, AIMD simulations are performed at constant density with a relatively small system size, and display large pressure fluctuations which yield uncertainties, typically of the order of ~ 1 GPa (inset of Figure 1).

The 1-bar bulk modulus K_T^0 (inverse of the isothermal compressibility) has been experimentally determined by sound-speed measurements for a number of mixtures.⁵⁴ It is found in excellent accordance with the ones resulting from the parameterization of the BMEoS using MD (e.g. in Table IV). K_T^0 consistently decreases with the cationic radius (Table III), unlike its P-dependence, K'^0 , that is almost invariant with chemical composition. Using a fusion curve analysis, Wang *et al.*⁵⁵ have constrained K'^0 for liquid K_2CO_3 , at pressure below 5 GPa, to 14.4 instead of 7.6 by MD. This disagreement can be explained by the indirect method used by the authors to obtain K'^0 from the Clapeyron curve. In this method (i) many thermodynamic data (which introduce uncertainties) are required, and (ii) the melting curve is not accurately known in the light of the differences between the studies of Klement and Cohen,³⁶ Wang *et al.*⁵⁵ and Li.⁵⁶

For carbonate mixtures, discrepancies on atmospheric density measurements can reach up to 5 %.^{10,37,44,45,47,48} The values from the study of Liu *et al.*³⁷ seem to be of first relevance since the authors have proven their reproducibility, have accounted for surface tension corrections and have tested their apparatus on standard liquids. The comparison of our MD results with their study shows the excellent transferability of our force field to the determination of the density of mixtures, as illustrated in Table IV on some selected compositions, namely the eutectic ternary mixture (Li_2CO_3 , Na_2CO_3 and K_2CO_3 in proportions 43.5:31.5:25 mol%,⁵⁷ LNKe) and a binary eutectic mixture (Li_2CO_3 and K_2CO_3 in proportions 62:38 mol%, LKe). Note that the density of mixtures follows an ideal mixing rule as it was reported by Liu *et al.*³⁷

$$n_{mix} = \frac{\sum_i x_i M_i}{\sum_i x_i \bar{V}_i} \quad , \quad (7)$$

where x_i is the molar fraction of species i of molar mass M_i and molar volume \bar{V}_i .

For the bulk modulus, an ideal mixing rule,

$$K_{mix} = \frac{\sum_i x_i \bar{V}_i}{\sum_i x_i \bar{V}_i / K_i} \quad , \quad (8)$$

is also verified (Table IV).

Therefore the use of the above mixing rules for the density and the bulk modulus, combined with the fact that K'^0 varies very little for the three end-members, leads to an accurate estimation of the density of mixtures in the system Li_2CO_3 – Na_2CO_3 – K_2CO_3 over a large range of $T - P$ conditions. For instance, considering the eutectic ternary mixture at 1500 K

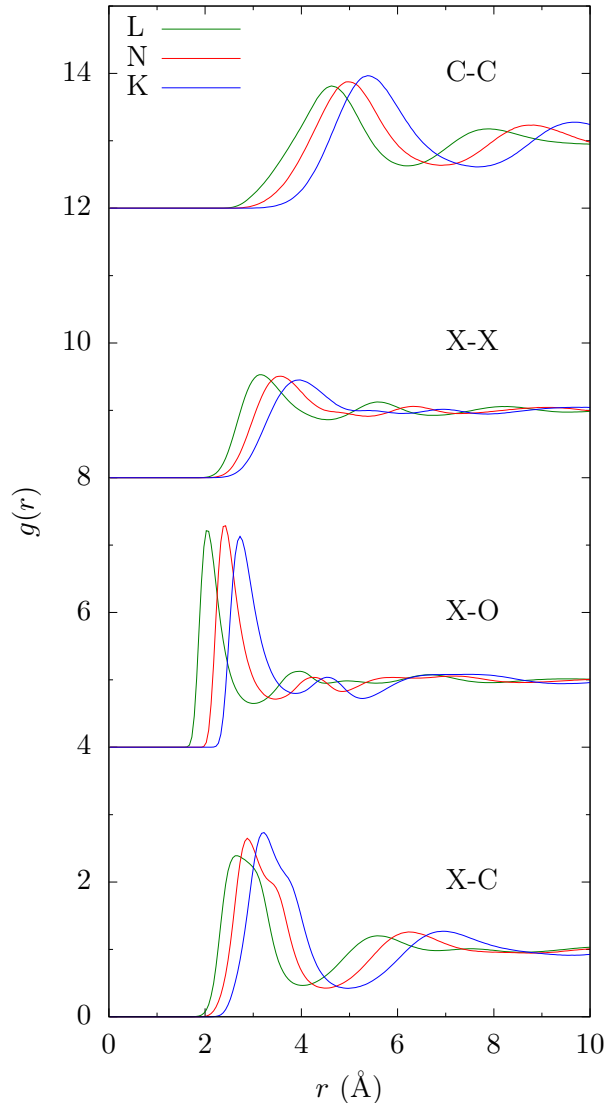


FIG. 2. Pair distribution functions C–C, X–X, X–O and X–C where C and O are carbon and oxygen atoms of the CO_3 groups and X=Li, Na or K, in Li_2CO_3 (L), Na_2CO_3 (N) and K_2CO_3 (K) at 1 bar and 1100 K. To help visualization the different PDFs were shifted vertically.

and 3 GPa, direct simulation gives a density of 2.15 g/cm^3 , while the use of equations (7) and (8), with $K^{\prime 0}$ in the range $7.6 - 8.5$ gives 2.16 g/cm^3 after using equation (4).

B. Evolution of the liquid structure with temperature and pressure

Despite their liquid nature, related to a long-range disorder, molten carbonates show a residual local ordering coming from the competition between ionic, dispersive and steric

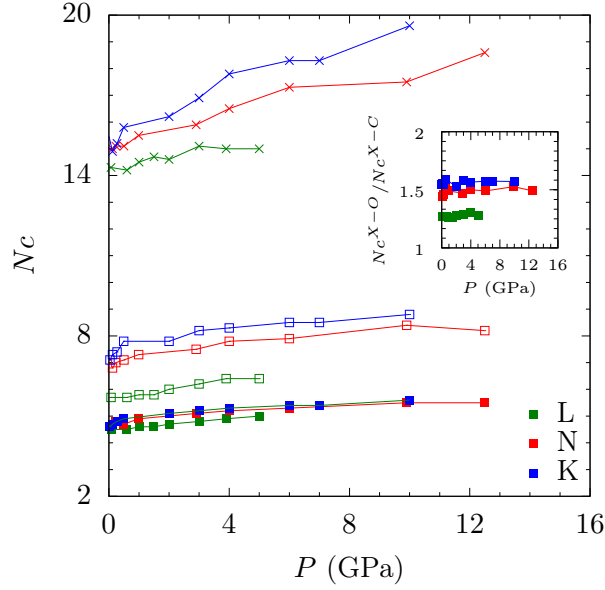


FIG. 3. Evolution with pressure of the coordination number of the C–C (crosses), X–C (plain squares) and X–O (empty square) pairs where X=Li, Na or K, in:

Li_2CO_3 (L) at 1140 K (0 GPa), 1200 K (0.1 GPa), 1350 K (0.5–1 GPa) and 1500 K (1.5–5 GPa),
 Na_2CO_3 (N) at 1200 K (0–1 GPa), 1650 K (3–6 GPa) and 2073 K (10–12.5 GPa),
 K_2CO_3 (K) at 1200 K (0–0.5 GPa), 1500 K (2–4 GPa), 1773 K (6 GPa) and 2073 K (7–10 GPa).

forces. Among these, the coulombic forces are essential as they impose an alternation of charges of opposite signs, as qualitatively confirmed by X-ray and neutron diffraction studies of molten carbonates.^{58,59} Thus the pair distribution functions (PDF) of X–C and C–C (where C is the carbon atom of CO_3 and X=Li, Na or K) are nearly in opposition of phase (Figure S1). However the structure of molten carbonates is complicated further, in comparison to simple ionic liquids, by the peculiar shape of the carbonate ion and by the anion-cation asymmetry of charge. The anion is surrounded by cations that subsequently attract carbonate anions into a second coordination shell. In turn the anions encircle the cation by pointing one or two oxygen atoms in its direction (see Table V). Actually the number of pointing O of each carbonate is barely sensitive to the size of the cation (~ 1.5 in each case, Table V). The number density progresses as follows at 1 bar and 1100 K: $\rho_{\text{Li}_2\text{CO}_3} = 24.4$ mol/L $>$ $\rho_{\text{Na}_2\text{CO}_3} = 18.7$ mol/L $>$ $\rho_{\text{K}_2\text{CO}_3} = 14.0$ mol/L. Therefore some structural features can be described as a simple homothetic transformation upon volumetric shrinkage from

	T	P	n	r^{X-X}	N_c^{X-X}	r^{C-C}	N_c^{C-C}	r^{X-C}	N_c^{X-C}	N_c^{C-X}	r^{X-O}	N_c^{X-O}	N_c^{O-X}
	(K)	(GPa)	(g/cm ³)	(Å)		(Å)		(Å)			(Å)		
Li ₂ CO ₃	1100	0	1.80	3.15	2.5	4.63	5.2	2.65	1.1	1.9	2.04	1.8	1.0
				4.75	12.4	6.22	14.3	4.03	4.5	9.0	3.03	5.9	3.9
Na ₂ CO ₃	1100	0	1.94	3.56	2.8	5.05	5.0	2.89	1.0	1.9	2.40	1.6	0.9
				5.38	13.7	6.90	15.0	4.48	4.7	9.4	3.48	6.8	4.6
K ₂ CO ₃	1100	0	1.89	3.94	2.9	5.40	4.8	3.25	1.1	2.3	2.73	1.5	1.2
				6.20	21.6	7.70	15.5	5.05	4.8	9.5	3.82	7.2	5.0

TABLE V. First neighbors in molten carbonates at 1100 K: distance r and coordination numbers N_c (with X=Li, Na or K and O and C are the oxygen and the carbon atom of CO₃, respectively). The first line reports values corresponding to the first maximum of the pair distribution function, the second line values evaluated at its first minimum.

K₂CO₃ to Li₂CO₃ (*e.g.* C–C pair on Figure 2). Interestingly, this simple behavior leads to a pseudo-ideal mixing rule of the cation-carbonate pair distribution functions. As a matter of fact the X–C PDFs associated with the pure end-members are quasi-identical to the ones observed in the corresponding mixtures (not shown).

According to the parametrization procedure we used, the PDFs from MD compare very well with the ones from AIMD (Figures S1a, S1b and S1c). Moreover the quality of the MD description is preserved at high $T - P$ as illustrated by the example of K₂CO₃ (Figure S1d). Actually the agreement between MD and AIMD is even better under pressure, except for the cation-cation (X–X) pair. With regard to the structural changes occurring with increasing pressure and temperature, it is noteworthy that on the $T - P$ range under study the local structure in the first shell depends very little on the temperature. For example, for K₂CO₃ at 4 GPa, the cation-oxygen N_c^{X-O} coordination number is 8.3 at 1500 K and 8.0 at 2073 K. Consequently the evolution of the coordination numbers N_c^{C-C} , N_c^{X-C} , N_c^{X-O} at increasing pressure and temperature can thus be assigned essentially to pressure (Figure 3). Surprisingly for all compositions, N_c^{X-O} evolves very little with pressure, it increases somewhat before levelling off. The ratio N_c^{X-O}/N_c^{X-C} plotted in the inset of Figure 3 is indicative of the orientation of the carbonate ions around the cations (there are 1.3 oxygen atoms pointing towards Li, \sim 1.5-1.6 towards Na and K) and is virtually independent of pressure. Although the pressure evolution of the coordination number of the C–C pair is a bit steeper, there is nothing remarkable in this evolution. This is at variance with the hypothesized reminiscence in the liquid structure of crystalline polymorphs at the corresponding pressure.⁶⁰ The

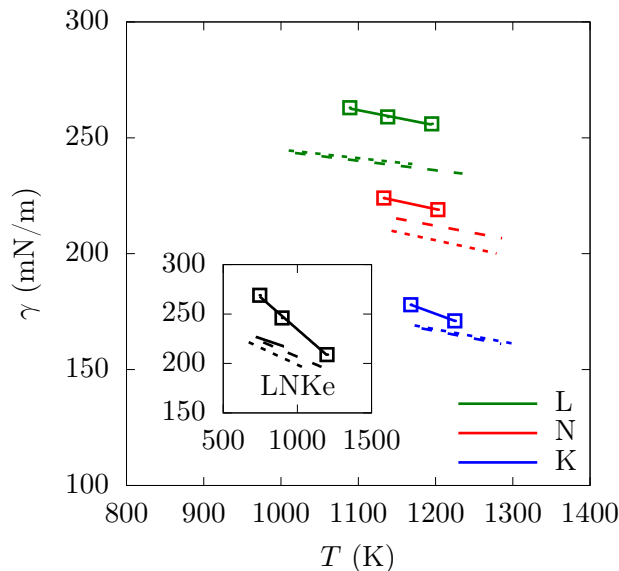


FIG. 4. Surface tension of the end-members Li_2CO_3 (L), Na_2CO_3 (N) and K_2CO_3 (K) calculated in MD (squares and plain lines as a guide to the eye) and measured experimentally (dashed line⁴³ and dotted line¹⁰). In the inset are the values for the ternary eutectic mixture (LNKe) calculated in MD (squares and plain lines) and measured experimentally (dashed line,⁴³ long dash⁶¹ and dotted line⁶²).

absence of a significant structural rearrangement of molten carbonates upon pressure should translate in smoothly varying transport coefficients over this pressure range.

Wilding *et al.*²⁰ have studied the structure of Na_2CO_3 at 1 bar and from 1100 to 1750 K, using MD and a FF adapted from Tissen and Janssen¹⁴. The authors assumed the formation of a low-dimensional network made of short carbonate-cation-carbonate chains argued by the presence of a shouldering in the first peak of $g_{\text{C-C}}(r)$ at 2.3 Å. Such a shouldering does not appear in our MD study, neither in the pair distribution function generated by AIMD. We believe that the aforementioned structural feature is due to the inaccuracy of the Janssen and Tissen¹³ force field, even when supplemented by an harmonic intramolecular potential for CO_3 , as used by Wilding *et al.*²⁰

C. Surface Tension

Surface tension can be evaluated by explicitly simulating the coexistence of the liquid with its vapor along a plane interface,^{63–65} and by calculating the long time limit of the average of some components of the stress tensor. More precisely, assuming that the z axis is perpendicular to the interface, the surface tension is given by:⁶⁶

$$\gamma = \lim_{t \rightarrow \infty} \gamma(t), \text{ with } \gamma(t) = \frac{L_z}{2} \left\langle \Pi_{zz} - \frac{1}{2} (\Pi_{xx} + \Pi_{yy}) \right\rangle, \quad (9)$$

where L_z is the length of the simulation box and Π_{xx} , Π_{yy} and Π_{zz} are the diagonal components of the stress tensor (see equation (13) in next section). We studied several compositions at different temperatures, but for the sake of clarity, we chose to present the result of only a few of them to picture the main trends (Figure 4). Our model recovers the right order of magnitude of experimental measurements of the surface tension, but seems to overestimate it systematically by 10–20 %. Moreover the temperature dependencies are satisfying although one notices an overestimation of the activation energy in the case of the LNKe mixture. The hierarchy between the different compositions is respected: the bigger the cation, the smaller the surface tension. Thus the surface tension decreases when the asymmetry of size between the cation and the anion decreases.⁶⁷

As mentioned above, the overestimation of the MD-calculated surface tension seems to be systematic (of the order of +10–15 % compared with Kojima⁴³). As our FF describes with accuracy the structure and the density as well as other properties (EoS, viscosity) which depend also strongly on cohesive forces⁶⁸ (see next section), this observation is somehow a surprise and raises concerns on possible systematic errors due to the simulation parameters. Some authors have pointed out that away from the interface the bulk, instead of showing isotropic properties, could wrongly contribute a non-zero amount to equation (9).⁶⁹ We tested the possible effect of this anomalous contribution in the case of the $\text{Li}_2\text{CO}_3\text{--Na}_2\text{CO}_3\text{--K}_2\text{CO}_3$ equimolar mixture at 900 K, by calculating the surface tension with a liquid depth increased by a factor 7 (z dimension from ~ 29 to 200 \AA), all else being equal. This resulted in a value of γ that is almost unchanged or maybe slightly decreased (from 239 ± 3 to 232 ± 6), which suggest a weak contribution of the bulk. We have tested several other parameters of the simulation which could affect the calculation of the surface tension namely, the size of the simulation box, the truncation cutoff of the van der Waals potential, and the parameters of the Ewald summation.⁶⁷ Although the calculated value changes a little

with these parameters, the variations seem too weak to explain the discrepancy with the experimental data (calculated values differ by less than 5 %). Larger scaling tests with much greater simulations boxes would be needed to completely rule out the role of finite size effect. However, it could be that our FF is less suitable to describe interfacial (rather than bulk) properties as it possibly fails to render some polarization effects. In any case, the discrepancies with the experiments we obtained are similar in magnitude with previous MD studies of ionic liquids.^{64,65} and this first attempt of simulating the surface tension of molten carbonates by MD leads to good qualitative predictions.

V. TRANSPORT PROPERTIES

Aiming at a systematic description of transport properties as a function of chemical composition, temperature and pressure, a large number of simulations were performed at different thermodynamic conditions for pure Li_2CO_3 , Na_2CO_3 and K_2CO_3 , as well as for some binary and ternary compositions. Each run was carried out in the NVE ensemble for a duration of 10–20 ns, which is sufficient to investigate the diffusive regime and to calculate accurately the self-diffusion coefficients D_s of each chemical species ($s = \text{Li}, \text{Na}, \text{K}$ and CO_3^{2-}), the electrical conductivity σ and the viscosity η , defined respectively by:^{70,71}

$$D_s = \lim_{t \rightarrow \infty} \frac{1}{6t} \frac{1}{N_s} \sum_{i=1}^{N_s} \left\langle |\mathbf{r}_i(t) - \mathbf{r}_i(0)|^2 \right\rangle , \quad (10)$$

$$\sigma = \lim_{t \rightarrow \infty} \frac{1}{6t} \frac{e^2}{k_B T V} \left\langle \left| \sum_{i=1}^N z_i (\mathbf{r}_i(t) - \mathbf{r}_i(0)) \right|^2 \right\rangle , \quad (11)$$

$$\eta = \lim_{t \rightarrow \infty} \frac{V}{k_B T} \int_0^t d\tau \left\langle \Pi_{\alpha\beta}(\tau) \cdot \Pi_{\alpha\beta}(0) \right\rangle , \quad (12)$$

where the off-diagonal pressure tensor components $\Pi_{\alpha\beta}(t)$, with $\alpha, \beta = x, y, z$ is given by:

$$\begin{aligned} \Pi_{\alpha\beta}(t) = \frac{1}{V} \sum_{i=1}^N \left(m_i v_{i\alpha}(t) v_{i\beta}(t) \right. \\ \left. + \sum_{j>i} r_{ij\alpha}(t) \cdot F_{ij\beta}(t) \right) , \end{aligned} \quad (13)$$

where N is the total number of ions in the simulation box of volume V , N_s the number of ions of species s , k_B the Boltzmann constant, e the elementary charge, m_i the mass of ion i and $\mathbf{r}_i(t)$ its position, $v_{i\alpha}(t)$ the component α of its velocity and $F_{ij\beta}(t)$ is the component β

of the force exerted by ion j on ion i , separated by distance $r_{ij}(t)$ at time t . The ensemble average $\langle \dots \rangle$ is taken over many time origins. The parameter z_i is the conduction charge of ion i (i.e. σ is effectively an ionic conductivity), chosen here as the formal charge, as it is usual for simple ionic liquids.⁷² Note that the optimal choice for the conduction charges, either formal or partial charges, is still an open question.^{21,22} The estimation of the self-diffusion coefficient D_s relies on an average over the N_s ions of a specific species s (sum $\sum_{i=1}^{N_s}$ in eq (10)), which ensures a small uncertainty of $\sim 1\%$. On the contrary, conductivity and viscosity are collective quantities that necessarily require a large number of atoms (and long time runs) to be correctly estimated with an error bar of 5–10 % in this study. For this reason, AIMD estimations are today only crude and suffer from high uncertainties. As a matter of fact, until now only two classical MD studies have provided estimations of the viscosity and electrical conductivity of carbonate melts, namely CaCO_3 ²¹ and the Li_2CO_3 – K_2CO_3 eutectic mixture (62:38 mol%) .²²

As usually observed for molten salts, the temperature dependence of the transport properties calculated by MD is well reproduced by an Arrhenius activation law. An activation volume V_a^X is introduced to take into account the pressure dependence of the physical quantity $X = D_s, \sigma$ and η , as in references 21 and 22. The following expressions are used:

$$D_s(P, T) = D_s^0 e^{-(E_a^{D_s} + PV_a^{D_s})/RT} , \quad (14)$$

$$\sigma(P, T) = \sigma^0 e^{-(E_a^\sigma + PV_a^\sigma)/RT} , \quad (15)$$

$$\eta(P, T) = \eta^0 e^{(E_a^\eta + PV_a^\eta)/RT} , \quad (16)$$

where E_a^X is the activation energy associated to the physical quantity X . The values of X^0 , E_a^X and V_a^X were determined by fitting the MD data for the three end-members Li_2CO_3 , Na_2CO_3 and K_2CO_3 (see Figures S3, S4, S5, S6 and S7). These values are given in Tables VI and VII, for D_s , σ and η and for the pressure and temperature range mentioned in Table III.

A crucial advantage of MD simulations is that all these transport coefficients are calculated in the same theoretical framework, which allows one to check the validity of approximate relations between electrical conductivity and self-diffusion coefficients (Nernst-Einstein equation) and between self-diffusion coefficients and viscosity (Stokes-Einstein equation). Furthermore, the role played by each chemical species and the correlations between their contributions to the transport properties can be easily investigated, as we shall see below.

	$D_{0,X}$ ($10^{-9}\text{m}^2/\text{s}$)	$E_a^{D_X}$ (kJ/mol)	$V_a^{D_X}$ (cm^3/mol)	D_{0,CO_3} ($10^{-9}\text{m}^2/\text{s}$)	$E_a^{D_{\text{CO}_3}}$ (kJ/mol)	$V_a^{D_{\text{CO}_3}}$ (cm^3/mol)
Li_2CO_3	176	32	$2.59-0.12P+0.0037P^2$	54	33	$2.4-0.18P-0.0145P^2$
Na_2CO_3	171	37	$4.2-0.25P+0.0081P^2$	82	39	$4.0-0.24P+0.0079P^2$
K_2CO_3	135	34	$5.2-0.43P+0.0179P^2$	78	38	$5.3-0.48P+0.0210P^2$

TABLE VI. Parameters of the Arrhenius activation law (14) obtained by the interpolation of all MD simulation points (with $X = \text{Li}, \text{Na}$ or K). P is in GPa.

A. Self-diffusion coefficients

We have first estimated the ion self-diffusion coefficients from our AIMD simulations, which were long enough to reach the diffusive regime. Thus at 1 bar we found $D_{\text{Na}} = 3.4 \pm 0.3 \cdot 10^{-9} \text{ m}^2/\text{s}$ and $D_{\text{CO}_3} = 1.5 \pm 0.3 \cdot 10^{-9} \text{ m}^2/\text{s}$ in Na_2CO_3 at 1140 K, and $D_{\text{K}} = 4.0 \pm 0.2 \cdot 10^{-9} \text{ m}^2/\text{s}$ and $D_{\text{CO}_3} = 1.8 \pm 0.3 \cdot 10^{-9} \text{ m}^2/\text{s}$ in K_2CO_3 at 1190 K, values which compare well with those obtained from MD (3.5 and 1.4, and 4.6 and 1.8, respectively) a finding which emphasizes the reliability of our empirical force field.

The only diffusivity data in molten alkali carbonates have been provided by Mills and Spedding^{73–75} who measured the self-diffusion coefficients of Na^+ , K^+ and CO_3^{2-} ions in pure, binary and ternary alkali carbonate melts, at atmospheric pressure only. Note that the self-diffusion coefficient of Li^+ has not been measured yet.

As illustrated in Figure 5, the agreement between MD and experimental results is satisfactory for D_{K} and D_{Na} , at least in the pure Na_2CO_3 melt and in the Na_2CO_3 – K_2CO_3 eutectic mixture (NKe), but the diffusivity of the CO_3^{2-} anion measured in various melt compositions is systematically higher by a factor of 1.5–3 than the one calculated by MD or by AIMD.

The activation energy (32–39 kJ/mol) depends slightly on the ion species and on the melt composition (Table VI and Figure 5), which is frequent in molten salts,⁷³ whereas the experimental values are between ~ 40 and 53 kJ/mol, with an error reportedly below 1 kJ/mol. Note that the activation energies (~ 36 kJ/mol) determined by the MD simulations of Corradini *et al.*²² for the molten LKe mixture are close to the ones we found in the same mixture (41 kJ/mol) as well as in the pure end-members (Table VI). However their values of D_{Li} and D_{K} are higher than ours, by a factor of ~ 1.5 .

General trends can be inferred from our MD simulations. By comparing the cation diffusivity in the three end-member compositions at a given temperature, the following hierarchy

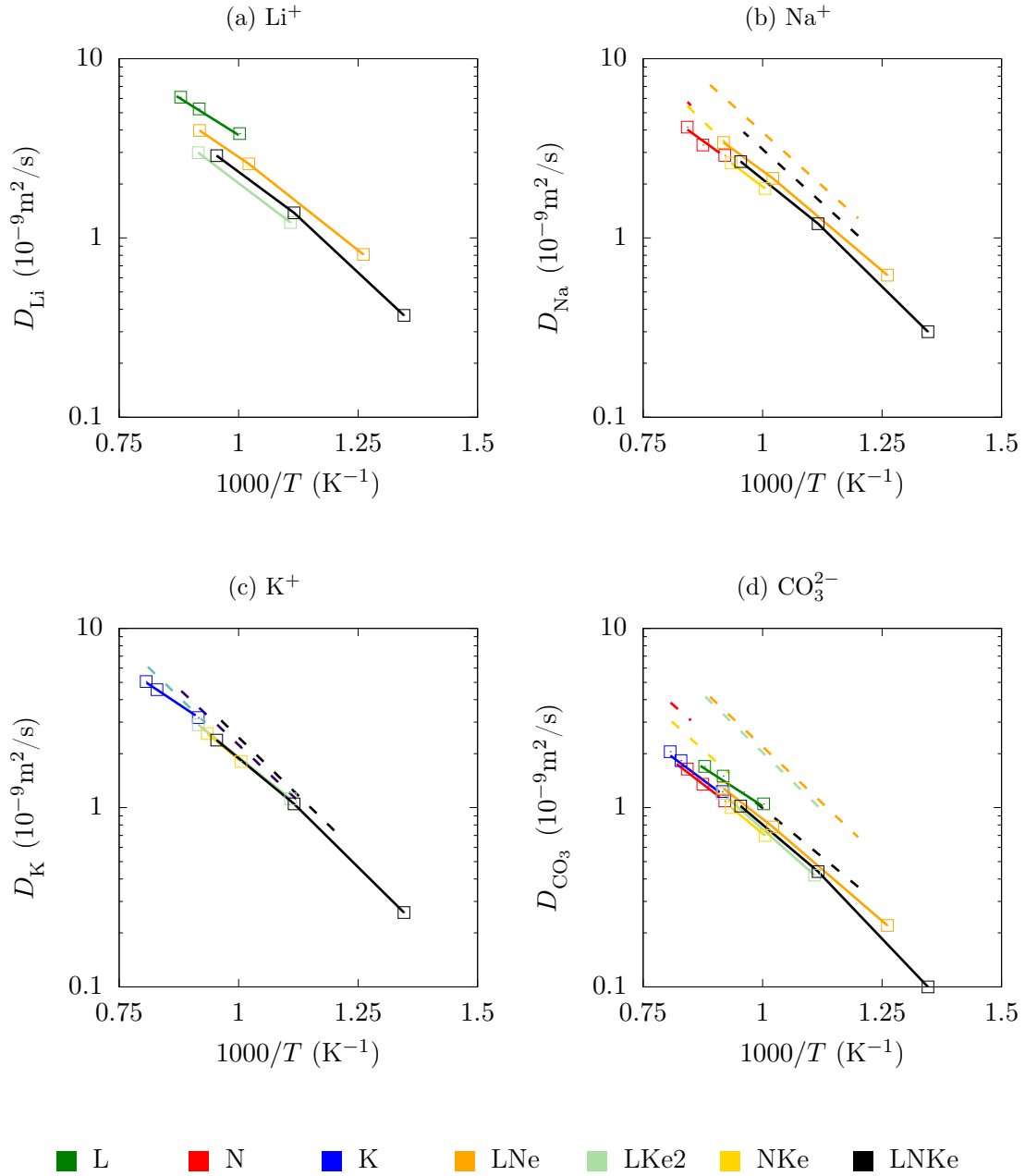


FIG. 5. Diffusion coefficient of ions in Li_2CO_3 (L), Na_2CO_3 (N), K_2CO_3 (K) and the eutectic mixtures Li_2CO_3 – Na_2CO_3 (LNe), Li_2CO_3 – K_2CO_3 (LKe2), Na_2CO_3 – K_2CO_3 (NKe) and Li_2CO_3 – Na_2CO_3 – K_2CO_3 (LNKe) calculated by MD (squares and plain lines as a guide to the eye) and experimentally measured by Spedding and Mills^{73,74} and Mills and Spedding⁷⁵ (dashed lines).

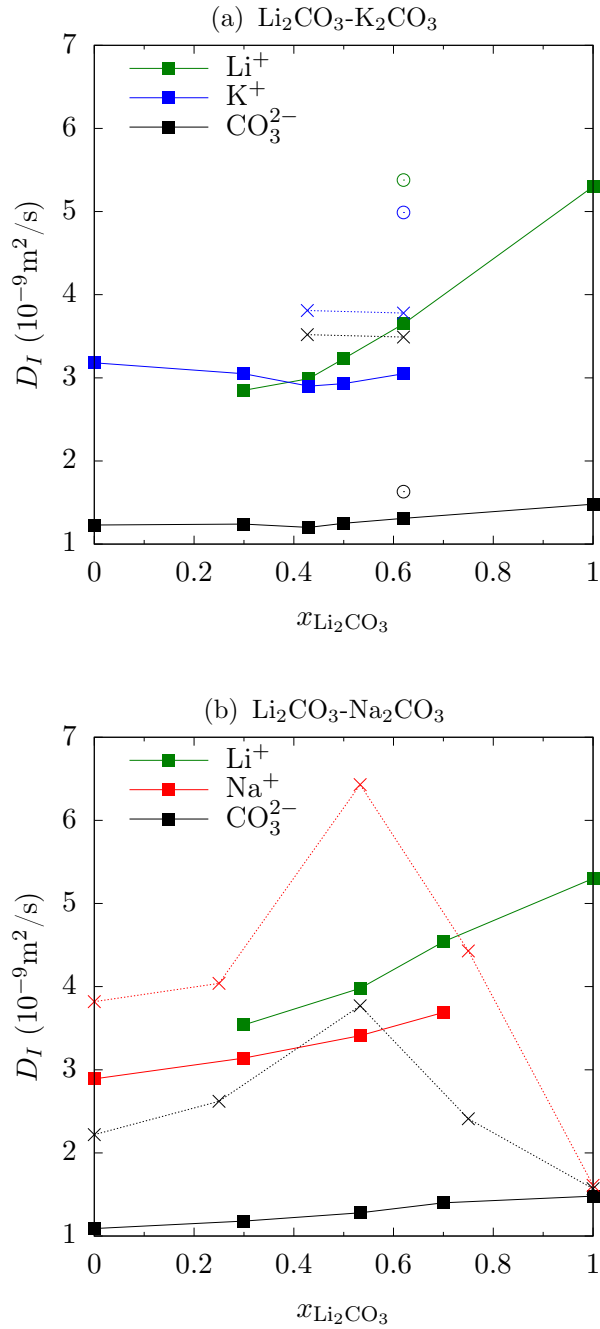


FIG. 6. Diffusion coefficients of ions in $\text{Li}_2\text{CO}_3\text{-K}_2\text{CO}_3$ and $\text{Li}_2\text{CO}_3\text{-Na}_2\text{CO}_3$ mixtures as a function of chemical composition ($x_{\text{Li}_2\text{CO}_3}$) at 1100 K and 1 bar: MD calculations of this study (plain squares and plain lines), experimental data^{73–75} (crosses and dashed lines) and MD data of Corradini *et al.*²² for the LKe mixture (empty circles). Note that no experimental data for the diffusion coefficient of Li^+ are available yet.

is found: $D_{\text{Li}} > D_{\text{Na}} > D_{\text{K}} > D_{\text{CO}_3}$, a behavior also found in experiments. As expected the largest ion CO_3^{2-} has the slowest diffusivity. This hierarchy of the self-diffusion coefficients with the ionic radius is also found in binary and ternary mixtures.

However upon mixing, the diffusion coefficient of an ion species may change with the melt composition. Hence, when diffusivity data are plotted as functions of the Li_2CO_3 molar content in mixtures $x_{\text{Li}_2\text{CO}_3}$, D_{Na} and D_{CO_3} display a maximum at the eutectic composition,^{73,74} as shown in Figure 6. According to Spedding and Mills,^{73,74} this feature could be due to a high level of structural disorder at the eutectic point, which could also explain the low melting temperature for this composition. At variance, our MD simulations do not display such a composition effect. Furthermore the microscopic structure, as expressed by the PDFs, does not seem more disordered at the eutectic point (compare Figure S1a to Figures S1b and S1c). In fact the calculated self-diffusion coefficients of Na^+ , CO_3^{2-} (and also Li^+) increase as the Li_2CO_3 content increases in the binary mixture (Figure 6). A different situation is observed in the Li_2CO_3 – K_2CO_3 mixture where D_{K} and D_{CO_3} are almost constant and exhibit a very slight minimum at 0.42, whereas D_{Li} is increasing with $x_{\text{Li}_2\text{CO}_3}$. A consequence is that $D_{\text{Li}} < D_{\text{K}}$ when $x_{\text{Li}_2\text{CO}_3} < 0.42$ (see Figure 6a). Thus, the major effect of mixing is that Na^+ and K^+ hinder the motion of the light Li^+ ion when $x_{\text{Li}_2\text{CO}_3}$ is low. Notice that the mobility measurements of Yang *et al.*⁷⁶ support the above findings. Those trends are also in accordance with previous numerical studies^{14,15,17–19} based on the force field by Janssen and Tissen.¹³

To our knowledge no diffusivity data are available under pressure. Our simulations predict an Arrhenius behavior according to equation (14). Thus the self-diffusion coefficients strongly decrease with pressure (see Figures S3, S4 and S5), a behavior also observed in the CaCO_3 melt.²¹ Concerning the comparison between MD and AIMD calculations we notice that at 6 GPa and 1773 K in the K_2CO_3 melt, the self-diffusion of K^+ and CO_3^{2-} calculated by MD are slightly lower than that obtained from AIMD: $D_{\text{K}} = 3.6$ and $5.0 \pm 0.5 \cdot 10^{-9}$ m²/s and $D_{\text{CO}_3} = 1.7$ and $3.5 \pm 0.5 \cdot 10^{-9}$ m²/s for MD and AIMD respectively, because densities are a little bit different in the two calculations (2.49 and 2.41 g/cm³ for MD and AIMD, respectively).

	σ_0 (S/m)	E_a^σ (kJ/mol)	V_a^σ (cm ³ /mol)	η_0 (Pa · s)	E_a^η (kJ/mol)	V_a^η (cm ³ /mol)
Li ₂ CO ₃	3295.3	18	1.1+0.166P-0.0148P ²	2.7×10 ⁻⁴	24	2.2+0.01P
Na ₂ CO ₃	2143.7	22	3.6-0.208P+0.0072P ²	2.5×10 ⁻⁴	27	3.5-0.10P
K ₂ CO ₃	1101.6	17	3.9-0.241P+0.0076P ²	2.2×10 ⁻⁴	27	4.7-0.20P

TABLE VII. Parameters of the Arrhenius activation laws (15) and (16) for electrical conductivity and viscosity, obtained by the interpolation of all MD simulation points. P is in GPa.

B. Electrical conductivity

The knowledge of the electrical conductivity of alkali carbonates is requisite for their industrial applications as electrolytes in fuel cell devices. Several experimental and numerical studies have been devoted to this issue. The measurements by Kojima *et al.* are broadly consistent with those reported by Janz¹⁰ for the end-members and various binary⁷⁷ and ternary⁴⁸ mixtures. Gaillard *et al.*⁶ also measured the electrical conductivity of the equimolar mixtures Na₂CO₃–K₂CO₃ (NK) and Li₂CO₃–Na₂CO₃–K₂CO₃ (LNK) at atmospheric pressure. Moreover the electrical conductivity of the LKe eutectic mixture was measured by Lair *et al.*⁵. The electrical conductivity data at atmospheric pressure are usually fitted by an Arrhenius law (see equation (15)). However some deviations were noticed at low temperature (< 973 K) by Kojima *et al.*, and for this reason they introduced a quadratic function of temperature (in $\log T$) to fit their data.

As shown in Figure 7, the electrical conductivity at 1 bar is negatively correlated to the cation size, as mentioned by Kojima *et al.*⁴⁸ and Sifré *et al.*¹¹ The agreement between MD calculations and the available 1-bar experimental data⁴³ is good for Li₂CO₃ and K₂CO₃ (Figure 7), within the error bars of both the simulations and the measurements (expected to be of the order of 10–15 %). Nevertheless the simulations underestimate somewhat the conductivities with respect to the experimental values of Kojima.⁴³ This discrepancy could be due to experimental inaccuracy. Indeed, the MD results are in very good agreement with the measurements of Gaillard *et al.*⁶ for the equimolar NK and LK systems and with those of Lair *et al.*⁵ for the LKe mixture, whose values are systematically below that of Kojima⁴³ (Figure 8).

The activation energy of calculated electrical conductivity is between 17 and 22 kJ/mol for the three end-members, which is slightly higher than the values found by Kojima⁴³ (15–

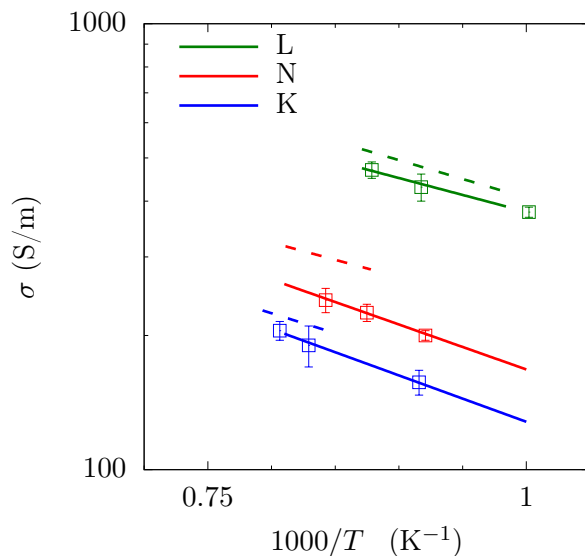


FIG. 7. Electrical conductivity at 1 bar from MD (squares and plain lines) and from experiments of Kojima⁴³ for Li_2CO_3 (L), Na_2CO_3 (N) and K_2CO_3 (K). The plain line is the Arrhenius activation law adjusted on the 1 bar MD values. It differs somewhat from the (P -dependent) law adjusted on all simulation points (Table VII), the parameters being: $\sigma_0(\text{L})=2170$ S/m, $E_a^\sigma(\text{L})=15$ kJ/mol, $\sigma_0(\text{N})=1700$ S/m, $E_a^\sigma(\text{N})=19$ kJ/mol, $\sigma_0(\text{K})=1400$ S/m, $E_a^\eta(\text{K})=20$ kJ/mol for Li_2CO_3 (L), Na_2CO_3 (N) and K_2CO_3 (K).

20 kJ/mol). In the LKe mixture at atmospheric pressure, E_a^σ calculated by Corradini *et al.*²² ($E_a = 20.22$ kJ/mol) is close to the ones measured by Kojima *et al.*⁷⁷ and Lair *et al.*⁵ ($E_a = 21.91$ kJ/mol for Kojima). As for the activation energies determined by Gaillard *et al.*⁶ in the equimolar Na_2CO_3 - K_2CO_3 and Li_2CO_3 - Na_2CO_3 - K_2CO_3 mixtures, they are higher, around 31 kJ/mol. Notice that the electrical conduction is a collective process including ion-ion correlations (see below). Therefore the activation energy associated to the electrical conductivity differs from that associated to the diffusion process (compare Table VII and Table VI)).

Up to a few kbars, the electrical conductivity depends weakly on pressure (see activation volumes in Table VII), whereas at higher pressures it significantly decreases with pressure (see Figure S6).

Assuming that the ions move independently from each other (the ion-ion cross correlations

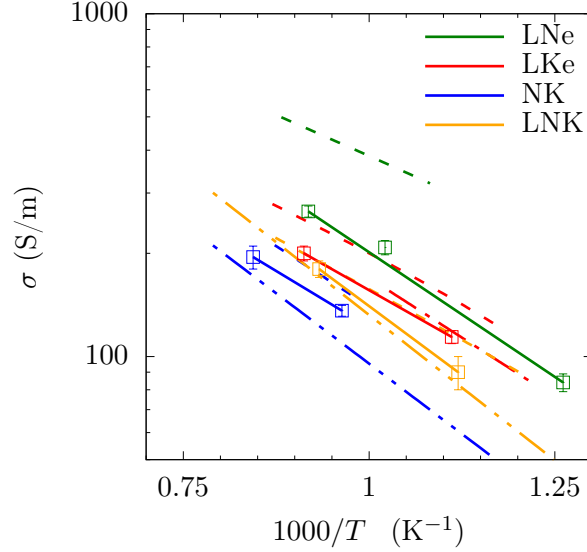


FIG. 8. Electrical conductivity at 1 bar from MD (squares and plain lines) and from experiments of Kojima⁴³ (dashed line), Lair *et al.*⁵ (long dashed and dotted lines) and Gaillard *et al.*⁶ (long dashed and double dotted lines) for several mixtures: eutectic Li_2CO_3 – Na_2CO_3 (56:44 mol.%, LNe), Li_2CO_3 – K_2CO_3 (62:38 mol.%, LKe) and equimolar Na_2CO_3 – K_2CO_3 (NK) and Li_2CO_3 – Na_2CO_3 – K_2CO_3 (LNK).

are then neglected), the "ideal" electrical conductivity, σ^{NE} is given by the Nernst-Einstein equation:

$$\begin{aligned} \sigma^{NE} &= \frac{e^2}{k_B T V} \sum_s N_s z_s^2 D_s \\ &= \frac{e^2}{k_B T V} \lim_{t \rightarrow \infty} \frac{1}{6t} \sum_s z_s^2 \sum_{i=1}^{N_s} \langle (\vec{\Delta}_i^{(s)}(t))^2 \rangle, \end{aligned} \quad (17)$$

where e is the elementary charge, k_B the Boltzmann constant and N_s , z_s and D_s are the number of ions, the conduction charge, equal to the formal charge here, and the self-diffusion coefficient of the chemical species $s = \text{Li}$, Na , K , and CO_3 respectively. In the right-hand side of equation (17), we made use of the definition (10) of the self-diffusion coefficient by writing $\vec{\Delta}_i^{(s)}(t) = \vec{r}_i^{(s)}(t) - \vec{r}_i^{(s)}(0)$.

The Haven ratio $H = \sigma/\sigma^{NE}$ is defined as the ratio of the exact electrical conductivity σ , here calculated using the Einstein relation (11) to the Nernst-Einstein conductivity (17). Note that the same electric charges are used (here, the formal ones) for evaluating σ and

σ^{NE} , therefore the value of H is independent of the charges assigned to the ions.

The value of H is usually less than 1 for molten salts, which is explained by the large contribution of the anticorrelations between ions of the same charge that tends to decrease the ideal conductivity σ^{NE} .⁷⁸ Simulations studies showed that $H \simeq 0.81$ for CaCO_3 melt,²¹ $H \sim 0.7$ for Li_2CO_3 - Na_2CO_3 mixtures¹⁹ and $H = 0.5$ - 1.0 for Li_2CO_3 - K_2CO_3 mixtures.¹⁸ However, the Haven ratio was found greater than 1 ($H = 1.8$) for LKe.²² Note that H may depend on pressure and temperature. In this work, we find a Haven ratio which is slightly greater than 1 for Li_2CO_3 (e.g. $H = 1.04$ at the melting point) and lower than 1 for Na_2CO_3 and K_2CO_3 (e.g. $H = 0.99$ and 0.94 , respectively, at the melting point). This ratio seems to depend slightly on temperature, and more appreciably on pressure, especially for Na_2CO_3 and K_2CO_3 . For instance, at 4 GPa and 1500 K (near the melting point) the H ratio of K_2CO_3 drops to 0.47 (Table VIII). The amplitude of H is often considered to be indicative of the degree of dynamic correlations between ions. So a value close to 1 should confirm the independence hypothesis of the Nernst-Einstein approximation. Nevertheless, we show below that such correlations are present in the melt even when $H \simeq 1$ and that the variations of H with chemical composition and thermodynamic conditions are due to subtle changes in dynamic correlations between ionic motions.

To better understand the role of ion-ion correlations it is suitable to develop the exact Einstein expression of the conductivity given by equation (11). Note that in this expression the charge displacement is squared as opposed to equation (10) that is the sum of each squared ionic displacement. After a few algebra equation (11) leads to the following expression

$$\begin{aligned}
\sigma &= \frac{e^2}{k_B T V} \lim_{t \rightarrow \infty} \frac{1}{6t} \left\langle \left(\sum_s \sum_{i=1}^{N_s} z_s \vec{\Delta}_i^{(s)}(t) \right)^2 \right\rangle \\
&= \frac{e^2}{k_B T V} \lim_{t \rightarrow \infty} \frac{1}{6t} \left\{ \sum_s z_s^2 \left(\sum_{i=1}^{N_s} \langle (\vec{\Delta}_i^{(s)}(t))^2 \rangle \right) \right. \\
&\quad + \sum_{i=1}^{N_s} \sum_{j \neq i}^{N_s} \langle \vec{\Delta}_i^{(s)}(t) \cdot \vec{\Delta}_j^{(s)}(t) \rangle \left. \right. \\
&\quad \left. + \sum_s \sum_{s' \neq s} z_s z_{s'} \left(\sum_{i=1}^{N_s} \sum_{j=1}^{N_{s'}} \langle \vec{\Delta}_i^{(s)}(t) \cdot \vec{\Delta}_j^{(s')}(t) \rangle \right) \right\}, \tag{18}
\end{aligned}$$

where N_s is the number of ions of species s , z_s is their charge and $\Delta_i^{(s)}(t)$ is the displacement of the ion i of species s . The first term in the RHS of the last equation is the Nernst-Einstein conductivity (17). We then get the expression of the Haven ratio in terms of the correlations

between ions:

$$H = \frac{\sigma}{\sigma^{NE}} = 1 + \sum_s H_s + \sum_s \sum_{s' \neq s} H_{ss'} \quad (19)$$

where H_s expresses the average cross correlations (through a scalar product) between the displacements of ions of species s :

$$H_s = \lim_{t \rightarrow \infty} \frac{1}{6t} \frac{z_s^2}{\sum_s N_s z_s^2 D_s} \sum_{i=1}^{N_s} \sum_{j \neq i}^{N_s} \langle \vec{\Delta}_i^{(s)}(t) \cdot \vec{\Delta}_j^{(s)}(t) \rangle, \quad (20)$$

and $H_{ss'}$ expresses the average cross correlations between the displacement of an ion i of species s and that of an ion j of another species s' :

$$H_{ss'} = \lim_{t \rightarrow \infty} \frac{1}{6t} \frac{z_s z_{s'}}{\sum_s N_s z_s^2 D_s} \sum_{i=1}^{N_s} \sum_{j=1}^{N_{s'}} \langle \vec{\Delta}_i^{(s)}(t) \cdot \vec{\Delta}_j^{(s')}(t) \rangle. \quad (21)$$

If the trajectories of the ions are independent from each other, $H_s = H_{ss'} = 0$ and the Nernst-Einstein approximation is recovered (*i.e.* $H = 1$). However, $H = 1$ doesn't imply that H_s and $H_{ss'} \sim 0$. For instance in Li_2CO_3 (see Table VIII), H is very close to 1 ($H = 1.04$) although $H_{\text{LiLi}} = 0.04$, $H_{\text{CO}_3} = -0.32$ and $H_{\text{LiCO}_3} = 0.32$. These results mean that the displacements of Li cations are mostly not correlated to each other, whereas those of CO_3 are negatively correlated to each other, *i.e.* two CO_3 have a high probability to move in opposite directions. At variance, the cation-anion correlation term $H_{\text{Li}_2\text{CO}_3} = 0.32$ is positive, meaning that cations and anions are also moving in the opposite direction (notice that in equation (21) $z_s z_{s'} < 0$). The net result is that H_{CO_3} and H_{LiCO_3} are canceling each other, leading to $H = 1 + H_{\text{Li}} = 1.04$. A different situation is observed with Na_2CO_3 and K_2CO_3 , for which the cancellation effect implies the three contributions H_X , H_{CO_3} and H_{XCO_3} . As a result the anion-cation correlations H_{XCO_3} contribute positively (0.48 for Na_2CO_3 and 0.46 for K_2CO_3), whereas the correlations between ions of the same species decrease H by a value of $H_X + H_{\text{CO}_3}$ (-0.49 for Na_2CO_3 and -0.52 for K_2CO_3), but these two contributions almost balance each other providing a Haven ratio $H = 1 + H_X + H_{\text{CO}_3} + H_{\text{XCO}_3}$ equal to ~ 1 (0.99 for Na_2CO_3 and 0.94 for K_2CO_3).

This approach can be carried out on other compositions, including binary and ternary mixtures. This issue will be more thoroughly discussed in a future paper. The conclusion we want to emphasize here is that the Nernst-Einstein relation leads to a reasonable estimation of the electrical conductivity, not because the underlying assumption (the ions move independently from one another) is valid, but because of a cancellation effect between ion-ion

	T (K)	P (GPa)	σ (S/m)	H	H_X	H_{CO_3}	H_{XCO_3}
Li_2CO_3	1100	0	430	1.04	0.04	-0.32	0.32
	1500	4.0	470	1.06	0.08	-0.34	0.32
Na_2CO_3	1140	0	224	0.99	-0.24	-0.25	0.48
	1500	4.0	154	0.80	-0.28	-0.31	0.39
K_2CO_3	1200	0	196	0.94	-0.38	-0.14	0.46
	1500	4.0	97	0.47	-0.38	-0.24	0.35

TABLE VIII. Haven ratio and its ionic contributions. Note that the error bar on these quantities is of the order of the error bar on the electrical conductivity: $\sim 5\text{--}10\%$.

correlations. Therefore the Nernst-Einstein relation must be carried with great caution, in particular when it is used to extract the ion diffusion coefficients.

C. Viscosity

Viscosity of molten alkali carbonates at ambient pressure has been measured since the sixties and critically reviewed by Janz.¹⁰ Its value stands between 3 and 30 mPa.s, depending on composition and temperature, as compared to 1 mPa.s, the typical viscosity of alkali chloride melts (NaCl at 1100 K) and liquid water (0.8 mPa.s at 300 K) at atmospheric pressure.

Afterwards, Sato *et al.* performed accurate measurements (errors within 3 %) of the viscosity of Li_2CO_3 , Na_2CO_3 and K_2CO_3 (as well as Rb_2CO_3 and Cs_2CO_3),⁷⁹ and of $Li_2CO_3\text{--}Na_2CO_3$ and $Li_2CO_3\text{--}K_2CO_3$ binary melts,⁸³ by using the oscillating method. However this technique may present some drawbacks (dependence on the apparatus, long time analysis...). On the other hand, the measurement of low viscosities at high temperature with the rotation method is tricky, but do not suffer from these disadvantages.⁸⁴ Using this approach with a high-temperature rheometer system, Kim *et al.*⁸⁴ obtained results that confirm those of Sato *et al.* for Li_2CO_3 , the $Li_2CO_3\text{--}K_2CO_3$ eutectic mixture of ratio 0.43:0.57 mol% (LKe2) and for the LNKe mixture, which has the lowest melting temperature (668 K).^{79,83} However Di Genova *et al.*⁸⁰ have recently applied a similar but improved method, as they claimed, and found viscosities systematically higher, by 30 to 100 %, compared to previous studies.

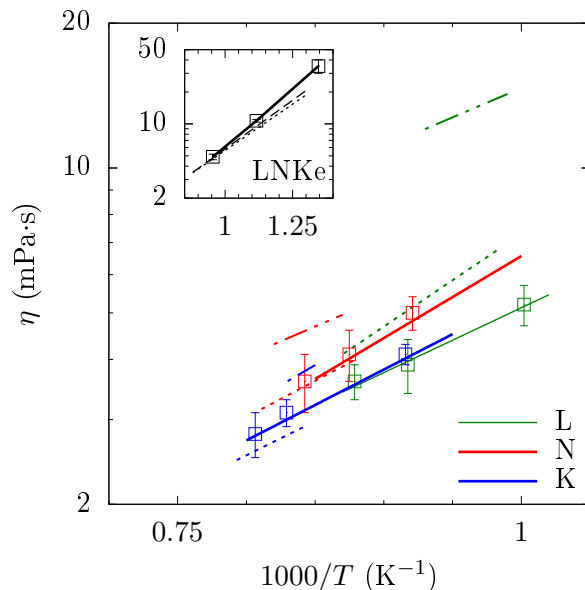


FIG. 9. Viscosity of the end-members Li_2CO_3 (L), Na_2CO_3 (N) and K_2CO_3 (K) at 1 bar, calculated by MD (squares and plain lines) and measured in references 10 and 79 (dotted line) and 80 (long dashed and double dotted lines). The plain line is the Arrhenius activation law adjusted on the 1-bar MD values. It differs somewhat from the law adjusted on all simulation points (Table VII), the parameters being: $\eta_0(\text{L}) = 1.8 \times 10^{-4}$ Pa.s, $E_a^\eta(\text{L}) = 26$ kJ/mol, $\eta_0(\text{N}) = 1.3 \times 10^{-4}$ Pa.s, $E_a^\eta(\text{N}) = 33$ kJ/mol, $\eta_0(\text{K}) = 1.8 \times 10^{-4}$ Pa.s, $E_a^\eta(\text{K}) = 28$ kJ/mol for Li_2CO_3 (L), Na_2CO_3 (N) and K_2CO_3 (K).

In the inset is plotted the viscosity of the eutectic ternary mixture (LNKe) calculated by MD (squares and plain line) and measured by An *et al.*⁸¹ (dotted line), indistinguishable from the data of Janz,¹⁰ and by Ejima⁸² (dashed line).

Concerning our simulations, they satisfactorily reproduce the experimental data of Sato⁷⁹ for Na_2CO_3 and K_2CO_3 and in particular the activation energy (see Figure 9). As mentioned above, there is a large disagreement between the experimental study of Di Genova *et al.*⁸⁰ and the one of Sato.⁷⁹ In particular the viscosity measured by Di Genova *et al.* for Li_2CO_3 is twice the one measured by Sato, and leads to a surprisingly large difference between the viscosity of Li_2CO_3 and those of Na_2CO_3 and K_2CO_3 . Indeed, such a contrasting behavior between the small Li^+ cation and the bigger Na^+ and K^+ cations, is not observed for other transport coefficients. As for our simulations of Li_2CO_3 , the calculated activation energy

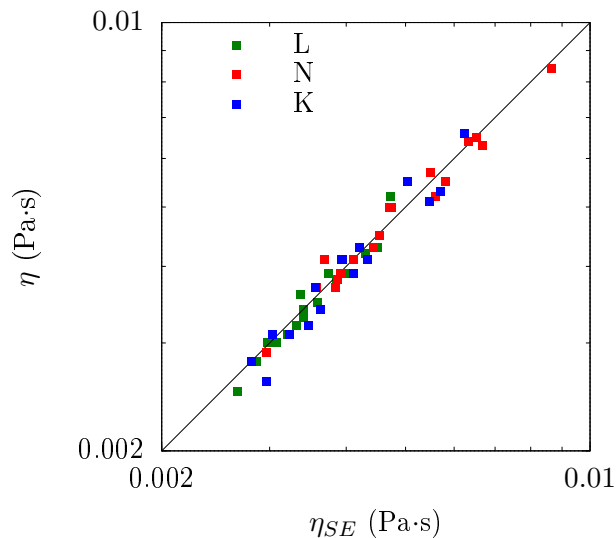


FIG. 10. Comparison of the viscosity calculated using the Green-Kubo formula, η , and the Stokes-Einstein equation, η_{SE} , for all T and P . The d parameter, figuring in equation (22) has been adjusted for Li_2CO_3 (L), Na_2CO_3 (N) and K_2CO_3 (K) to 1.6, 2.2 and 2.4 Å respectively, so as to align the data on the $\eta = \eta_{SE}$ bisector (black line).

is compatible with the data but the magnitude of the viscosity is ~ 15 % lower than that measured by Sato *et al.*⁸³ and Kim *et al.*⁸⁴ This result could be explained by the neglecting of some electronic effects (*e.g.* polarizability) in our model. Still, with regard to the viscosity of Na_2CO_3 and K_2CO_3 the calculated values are very close to the experimental ones (within the experimental uncertainties).

On the inset of Figure 9 the measured and calculated viscosity of the Li_2CO_3 - Na_2CO_3 - K_2CO_3 eutectic mixture is also shown. A good agreement is found with both the reference data of Janz¹⁰ and Ejima⁸² and the recent measurements of An *et al.*,⁸¹ emphasizing the ability of our force field to model the contribution of all the ions in mixtures. With regard to the LKe mixture, the viscosity estimated by our MD simulations is 10–30 % higher than the one measured by Sato *et al.*,⁸³ with an activation energy equal to 42.6 kJ/mol (as compared to 34 kJ/mol), whereas the one calculated by Corradini *et al.*²² is by 20–30 % lower (with a lower activation energy of 29.6 kJ/mol).

Like the other transport coefficients, the evolution of viscosity with temperature at high

pressure is conveniently reproduced by an Arrhenius activation law given by equation (16), the parameters of which are given in Table VII. As shown in Figure S7 for low and moderate pressures ($P < 1$ GPa), the viscosity depends almost exclusively on temperature. However beyond a few GPa, the weight of the activation volume V_a^η is no longer negligible. Very recently, Stagno *et al.*⁸⁵ reported viscosity measurements for Na_2CO_3 in the 1.7–4.6 GPa pressure range, that are in agreement with our calculations (deviation within 0–50 %, Figure S7b).

Interestingly, the activation energy differs from that of electrical conductivity (Table VII). The viscosity is indeed dominated by the motion of slow ions, as opposed to the electrical conductivity which is controlled by the fastest species. Still the viscosity can be described fairly well by the phenomenological Stokes-Einstein equation:

$$\eta_{SE} = \frac{k_B T}{2\pi D d} \quad , \quad (22)$$

using the arithmetic mean of the diffusion coefficients, $D = \sum_s x_s D_s / \sum_s x_s$ where x_s is the molar fraction of ion of species s in the melt, and d is the hydrodynamic diameter of the diffusing ions. By choosing $d = 1.6, 2.2$ and 2.4 Å for $\text{Li}_2\text{CO}_3, \text{Na}_2\text{CO}_3$ and K_2CO_3 respectively, we found that the behavior of the MD-calculated viscosity with pressure and temperature is correctly reproduced by equation (22) as demonstrated by Figure 10.

Finally, we find that the electrical conductivity σ (in S/m) and the viscosity η (in Pa.s) are related by the following empirical formula:

$$\sigma = \frac{A}{\eta^{0.8}} \quad , \quad (23)$$

where $A = 5.375, 2.615$ and 1.825 for $\text{Li}_2\text{CO}_3, \text{Na}_2\text{CO}_3$ and K_2CO_3 respectively (Figure S8). A comparable relation between these two transport properties has been also highlighted from experimental data of various melt compositions.^{11,21} The simple relations between D, σ and η can be very useful to infer one of these quantities from the others. They also show that these transport properties are essentially ruled by the diffusion of all ionic species in carbonate melts. This is in contrast with silicate melts whose viscosity is governed by the relaxation time of the Si-O bonds network, whereas the conductivity is mainly controlled by the mobility of network modifier elements, at least at low temperature near the melting point.

VI. CONCLUSION

We have studied the thermodynamics (equation of state and surface tension), the microscopic structure and the transport properties (diffusion coefficients, electrical conductivity and viscosity) of molten alkali carbonates (Li_2CO_3 , Na_2CO_3 , K_2CO_3 and some of their binary and ternary mixtures) in the $T - P$ range: $\sim 1100\text{--}2100$ K, $0\text{--}15$ GPa. For this we have developed an empirical force field using benchmark data from experiments (density and compressibility of the end-members at 1 bar) and from AIMD simulations (microscopic structure of four liquids). The density and compressibility data for binary and ternary mixtures that were not used in the FF parameterization procedure are also very well reproduced. We also showed for the end-members that the density of the crystalline phase at room conditions could be obtained with a good accuracy. Furthermore, the global agreement between the MD results and the full set of experimental data (thermodynamics and transport coefficients) is very satisfying. This gives consistent evidence for the ability of the FF to be transferable in terms of composition and thermodynamic conditions. In this respect we believe it is a significant improvement compared to the previously existing force fields for molten alkali carbonates.

Using this force field, the equation of state of the end-members was first evaluated and modeled by a third-order Birch-Murnaghan formula. Next we have shown that mixtures behave ideally regarding the density and the compressibility. The analysis of the PDFs showed that the microscopic structure is that of an ionic liquid and the only modification we could identify upon increasing pressure was a compaction effect. As for the transport properties (diffusion coefficients, electrical conductivity and viscosity), they evolve smoothly (Arrhenius-like) over the studied $T - P$ domain.

Moreover, for the first time the surface tension of molten carbonates was calculated using MD. Although the calculated values are systemically higher than the experimental values published in the literature, the discrepancy is moderate ($\sim +15\%$), as observed in previous numerical studies dealing with ionic liquids, and could be due to computational uncertainties (size effects).

Finally we discussed the significance of the Nernst-Einstein and the Stokes-Einstein equations, that relate the diffusion coefficients to the electrical conductivity and to the viscosity, respectively. We showed that, by using *ad hoc* parameters, both formula lead to reasonable

values. However they are not always representative of the transport mechanism itself. In particular we have demonstrated that the fairly good predictions provided by the Nernst-Einstein equation result from a partial canceling of interionic dynamic correlations.

SUPPLEMENTARY MATERIAL

See supplementary material for comparisons of the PDFs issued by MD and by AIMD simulations, a summary of all calculated properties with their uncertainties, plots of the evolution of these properties with T and P , convergence plots of the correlation functions and details on the AIMD simulations including an example input file.

ACKNOWLEDGMENTS

The research leading to these results has received funding from the Région Ile-de-France and the European Communitys Seventh Framework Program (FP7/2007-2013) under Grant agreement (ERC, N° 279790). The authors acknowledge GENCI for HPC resources (Grant No. 2015-082309).

REFERENCES

- ¹D. Chery, V. Lair, and M. Cassir, *Electrochim. Acta* **160** (2015).
- ²D. Chery, V. Lair, and M. Cassir, *Front. Energy Res.* **3** (2015).
- ³M. Cassir, S. McPhail, and A. Moreno, *Int. J. Hydrogen Energy* **37** (2012).
- ⁴M. Cassir, A. Ringued, and V. Lair, in *Molten Salts Chemistry*, edited by F. Lantelme and H. Groult (Elsevier, Oxford, 2013).
- ⁵V. Lair, V. Albin, A. Ringuedé, and M. Cassir, *Int. J. Hydrogen Energy* **37** (2012).
- ⁶F. Gaillard, M. Malki, G. Iacono-Marziano, M. Pichavant, and B. Scaillet, *Science* **322** (2008).
- ⁷R. Dasgupta and M. M. Hirschmann, *Earth Planet. Sci. Lett.* **298** (2010).
- ⁸R. Dasgupta, *Rev. Mineral. Geochem.* **75** (2013).
- ⁹T. Hammouda and S. Keshav, *Chem. Geol.* **418** (2015).
- ¹⁰G. J. Janz, *J. Phys. Chem. Ref. Data* **Suppl. 2** (1988).
- ¹¹D. Sifré, L. Hashim, and F. Gaillard, *Chem. Geol.* **418** (2015).

- ¹²Y. Kono, C. Kenney-Benson, D. Hummer, H. Ohfuji, C. Park, G. Shen, Y. Wang, A. Kavner, and C. E. Manning, *Nat. Commun.* **5** (2014).
- ¹³G. Janssen and J. Tissen, *Mol. Simul.* **5** (1990).
- ¹⁴J. Tissen and G. Janssen, *Mol. Phys.* **71** (1990).
- ¹⁵J. Tissen and G. Janssen, *Mol. Phys.* **82** (1994).
- ¹⁶J. Habasaki, *Mol. Phys.* **69** (1990).
- ¹⁷T. Koishi, S. Kawase, S. Tamaki, and T. Ebisuzaki, *J. Phys. Soc. Jpn.* **69** (2000).
- ¹⁸M. F. Costa, *J. Mol. Liq.* **138** (2008).
- ¹⁹A. Ottochian, C. Ricca, F. Labat, and C. Adamo, *J. Mol. Model.* **22** (2016).
- ²⁰M. C. Wilding, M. Wilson, O. L. G. Alderman, C. Benmore, J. K. R. Weber, J. B. Parise, A. Tamalonis, and L. Skinner, *Sci. Rep.* **6** (2016).
- ²¹R. Vuilleumier, A. Seitsonen, N. Sator, and B. Guillot, *Geochim. Cosmochim. Acta* **141** (2014).
- ²²D. Corradini, F.-X. Coudert, and R. Vuilleumier, *J. Chem. Phys.* **144** (2016).
- ²³E. Desmaele, *Physicochemical Properties of Molten Carbonates from Atomistic Simulations*, Ph.D. thesis, Sorbonne Université (2017).
- ²⁴J. VandeVondele, M. Krack, F. Mohamed, M. Parrinello, T. Chassaing, and J. Hutter, *Comput. Phys. Commun.* **167** (2005).
- ²⁵G. Lippert, J. Hutter, and M. Parrinello, *Mol. Phys.* **92** (1997).
- ²⁶J. VandeVondele and J. Hutter, *J. Chem. Phys.* **127** (2007).
- ²⁷S. Goedecker, M. Teter, and J. Hutter, *Phys. Rev. B* **54** (1996).
- ²⁸C. Hartwigsen, S. Goedecker, and J. Hutter, *Phys. Rev. B* **58** (1998).
- ²⁹M. Krack, *Theor. Chem. Acc.* **114** (2005).
- ³⁰A. D. Becke, *Phys. Rev. A* **38** (1988).
- ³¹C. Lee, W. Yang, and R. G. Parr, *Phys. Rev. B* **37** (1988).
- ³²S. Grimme, J. Antony, S. Ehrlich, and H. Krieg, *The Journal of Chemical Physics* **132**, 154104 (2010).
- ³³S. Nosé, *Mol. Phys.* **52** (1984).
- ³⁴S. Nosé, *J. Chem. Phys.* **81** (1984).
- ³⁵A. K. van Groos, *Am. Mineral.* **75** (1990).
- ³⁶W. Klement and L. H. Cohen, *Ber. Bunsenges. Phys. Chem.* **79** (1975).
- ³⁷Q. Liu and R. Lange, *Contrib. Mineral. Petrol.* **146** (2003).

- ³⁸W. Smith and T. Forester, *J. Mol. Graphics* **14** (1996).
- ³⁹S. M. Antao and I. Hassan, *Can. Mineral.* **48** (2010).
- ⁴⁰Y. Idemoto, J. W. Richardson, N. Koura, S. Kohara, and C.-K. Loong, *J. Phys. Chem. Solids* **59** (1998).
- ⁴¹A. Arakcheeva, L. Bindi, P. Pattison, N. Meisser, G. Chapuis, and I. Pekov, *Am. Mineral.* **95** (2010).
- ⁴²B. M. Gatehouse and D. J. Lloyd, *J. Chem. Soc., Dalton Trans* (1973).
- ⁴³T. Kojima, *Physical and Chemical Properties of Molten Carbonates*, Ph.D. thesis, Kobe University (2009).
- ⁴⁴G. J. Janz and M. R. Lorenz, *J. Electrochem. Soc.* **108** (1961).
- ⁴⁵P. L. Spedding, *J. Electrochem. Soc.* **117** (1970).
- ⁴⁶Z. Hong-Min, T. Saito, Y. Sato, T. Yamamura, K. Shimakage, and T. Ejima, *J. Japan Inst. Metals* **55** (1991).
- ⁴⁷T. Kojima, Y. Miyazaki, K. Nomura, and K. Tanimoto, *J. Electrochem. Soc.* **150** (2003).
- ⁴⁸T. Kojima, Y. Miyazaki, K. Nomura, and K. Tanimoto, *J. Electrochem. Soc.* **155** (2008).
- ⁴⁹D. P. Dobson, A. P. Jones, R. Rabe, T. Sekine, K. Kurita, T. Taniguchi, T. Kondo, T. Kato, O. Shimomura, and S. Urakawa, *Earth Planet. Sci. Lett.* **143** (1996).
- ⁵⁰Q. Liu, T. J. Tenner, and R. A. Lange, *Contrib. Mineral. Petrol.* **153** (2007).
- ⁵¹F. Birch, *Phys. Rev.* **71** (1947).
- ⁵²S. M. Rigden, T. J. Ahrens, and E. M. Stolper, *J. Geophys. Res.* **94** (1989).
- ⁵³B. Guillot and N. Sator, *Geochim. Cosmochim. Acta* **71** (2007).
- ⁵⁴M. C. O’Leary, R. A. Lange, and Y. Ai, *Contrib. Mineral. Petrol.* **170** (2015).
- ⁵⁵M. Wang, Q. Liu, T. Inoue, B. Li, S. Pottish, J. Wood, C. Yang, and R. Tao, *J. Mineral. Petrol. Sci.* **111** (2016).
- ⁵⁶Z. Li, *Melting and Structural Transformations of Carbonates and Hydrous Phases in Earth’s Mantle.*, Ph.D. thesis, University of Michigan (2015).
- ⁵⁷H. C. Maru, in *Molten Salt Techniques: Volume 2* (Springer US, Boston, MA, 1984).
- ⁵⁸J. Zarzycki, *Discuss. Faraday Soc.* **32** (1961).
- ⁵⁹S. Kohara, Y. S. Badyal, N. Koura, Y. Idemoto, S. Takahashi, L. A. Curtiss, and M.-L. Saboungi, *J. Phys.: Condens. Matter* **10** (1998).
- ⁶⁰J. Hudspeth, C. Sanloup, and Y. Kono, *Geochem. Persp. Lett.* **7** (2018).
- ⁶¹K. Igarashi, K. Tajiri, T. Asahina, and M. Kosaka, *Z. Naturforsch.* **47a** (1992).

- ⁶²A. Ward and G. Janz, *Electrochim. Acta* **10** (1965).
- ⁶³J. Alejandre, D. J. Tildesley, and G. A. Chapela, *J. Chem. Phys.* **102** (1995).
- ⁶⁴A. Aguado and P. A. Madden, *J. Chem. Phys.* **117** (2002).
- ⁶⁵M. Salanne, C. Simon, P. Turq, and P. A. Madden, *C. R. Chim.* **10** (2007).
- ⁶⁶J. G. Kirkwood and F. P. Buff, *J. Chem. Phys.* **17** (1949).
- ⁶⁷M. González-Melchor, P. Orea, J. López-Lemus, F. Bresme, and J. Alejandre, *J. Chem. Phys.* **122** (2005).
- ⁶⁸A. Marchand, J. H. Weijs, J. H. Snoeijer, and B. Andreotti, *Am. J. Phys* **79** (2011).
- ⁶⁹A. Sanmartn Pensado, P. Malfreyt, and A. A. H. Pdua, *The Journal of Physical Chemistry B* **113**, 14708 (2009).
- ⁷⁰M. P. Allen and D. J. Tildesley, *Computer Simulation of Liquids* (Clarendon Press, New York, NY, USA, 1989).
- ⁷¹B. Hess, *J. Chem. Phys.* **116** (2002).
- ⁷²E. M. Adams, I. R. McDonald, and K. Singer, *Proc. R. Soc. A* **357** (1977).
- ⁷³P. L. Spedding and R. Mills, *J. Electrochem. Soc.* **112** (1965).
- ⁷⁴P. L. Spedding and R. Mills, *J. Electrochem. Soc.* **113** (1966).
- ⁷⁵R. Mills and P. L. Spedding, *J. Chem. Phys.* **70** (1966).
- ⁷⁶C. Yang, R. Takagi, K. Kawamura, and I. Okada, *Electrochim. Acta* **32** (1987).
- ⁷⁷T. Kojima, Y. Miyazaki, K. Nomura, and K. Tanimoto, *J. Electrochem. Soc.* **154** (2007).
- ⁷⁸H. K. Kashyap, H. V. Annapureddy, F. O. Raineri, and C. J. Margulis, *J. Chem. Phys. B* **115** (2011).
- ⁷⁹Y. e. a. Sato, *Netsu Bussei* **13** (1999).
- ⁸⁰D. Di Genova, C. Cimorelli, K.-U. Hess, and D. B. Dingwell, *Am. Mineral.* **101** (2016).
- ⁸¹X. An, J. Cheng, P. Zhang, Z. Tang, and J. Wang, *Faraday Discuss.* **190** (2016).
- ⁸²T. e. a. Ejima, *J. Chem. Eng. Data* **32** (1987).
- ⁸³Y. Sato, T. Yamazaki, H. Kato, H. Zhu, M. Hoshi, and T. Yamamura, *Netsu Bussei* **13** (1999).
- ⁸⁴S. W. Kim, K. Uematsu, K. Toda, and M. Sato, *J. Ceram. Soc. Jpn.* **123** (2015).
- ⁸⁵V. Stagno, V. Stopponi, Y. Kono, C. E. Manning, and T. Irifune, *Chem. Geol.* (*in press*).

**Supplementary Material for "Atomistic simulations of molten carbonates:
thermodynamic and transport properties of the $\text{Li}_2\text{CO}_3\text{-Na}_2\text{CO}_3\text{-K}_2\text{CO}_3$ system"**

Elsa Desmaele,^{1, a)} Nicolas Sator,¹ Rodolphe Vuilleumier,² and Bertrand Guillot^{1, b)}

¹⁾*Sorbonne Université, CNRS, Laboratoire de Physique*

Théorique de la Matière Condensée, LPTMC, F75005, Paris,

France

²⁾*PASTEUR, Département de chimie, École normale supérieure,*

PSL University, Sorbonne Université, CNRS, 75005 Paris,

France

(Dated: 7 February 2019)

^{a)}Electronic mail: elsa.desmaele@gmail.com

^{b)}Electronic mail: guillot@lptmc.jussieu.fr

CONTENTS

List of Figures	2
List of Tables	2
CP2K input file example	21
References	26

LIST OF FIGURES

S1	Pair distribution functions from MD and AIMD	5
S2	Compression isotherms for Li_2CO_3 , Na_2CO_3 and K_2CO_3	6
S3	Diffusion coefficients in Li_2CO_3 as a function of T and P	7
S4	Diffusion coefficients in Na_2CO_3 as a function of T and P	7
S5	Diffusion coefficients in K_2CO_3 as a function of T and P	8
S6	Electrical conductivity as a function of T and P	9
S7	Viscosity as a function of T and P	10
S8	Electrical conductivity as a function of viscosity	11
S9	Method for the calculation of the electrical conductivity	12
S10	Method for the calculation of the viscosity	13
S11	Uncertainties on the electrical conductivity and on the viscosity as standard deviations using block averaging	14

LIST OF TABLES

S1	Details of the AIMD simulations.	4
S2	Crystal structure parameters	4
S3	Summary of the calculated properties for Li_2CO_3	15
S4	Summary of the calculated properties for Na_2CO_3	16
S5	Summary of the calculated properties for K_2CO_3	17
S6	Summary of the calculated for binary mixtures	18
S7	Summary of the calculated for ternary mixtures	19

S8	Summary of the calculated surface tension for Li_2CO_3 , Na_2CO_3 and K_2CO_3 .	19
S9	Summary of the calculated surface tension for binary and ternary mixtures . .	20

	N	t_{sim} (ps)	n (g/cm ³)	T (K)	$\langle P \rangle$ (GPa)
Na ₂ CO ₃	768	48.0	1.97	1140	0 ± 0.5
K ₂ CO ₃	204	13.2	1.90	1190	0 ± 0.5
	204	24.0	2.41	1773	6 ± 1.5

TABLE S1. Details of the AIMD simulations.

	n (g/cm ³)	a (Å)	b (Å)	c (Å)	β (°)
Li ₂ CO ₃	2.12	8.77	5.09	6.16	119.7
Exp. ^{S1}	2.10	8.36	4.97	6.19	114.7
Na ₂ CO ₃	2.50	9.08	5.31	5.97	101.9
Exp. ^{S2}	2.54	8.91	5.24	6.05	101.4
K ₂ CO ₃	2.45	5.67	9.98	6.83	100.2
Exp. ^{S3}	2.47	5.64	9.84	6.87	98.7

TABLE S2. Crystal structure parameters for monoclinic Li₂CO₃, Na₂CO₃ and K₂CO₃ (300 K, 1 bar) from the experimental literature (Exp.) and calculated by anisotropic MD simulations (*NST* ensemble) starting from the experimentally determined structures.

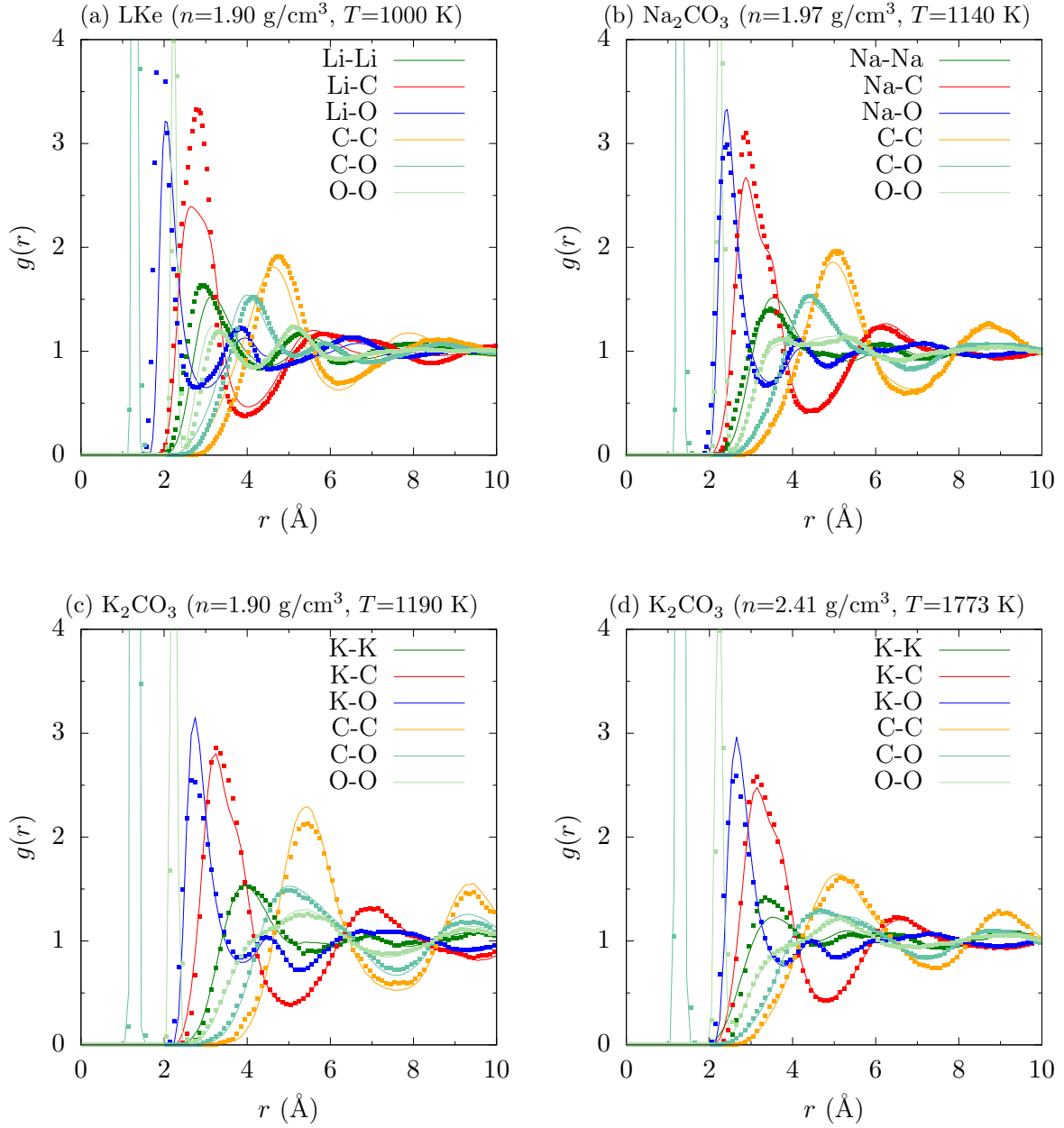


FIG. S1. Pair distribution functions obtained by MD (full line) and AIMD (squares). Chemical compositions, temperatures and densities are mentioned above the figures. In the case of panel (a), only $g(r)$ associated with the Li_2CO_3 component of the Li_2CO_3 - K_2CO_3 eutectic mixture (LKe) are plotted.

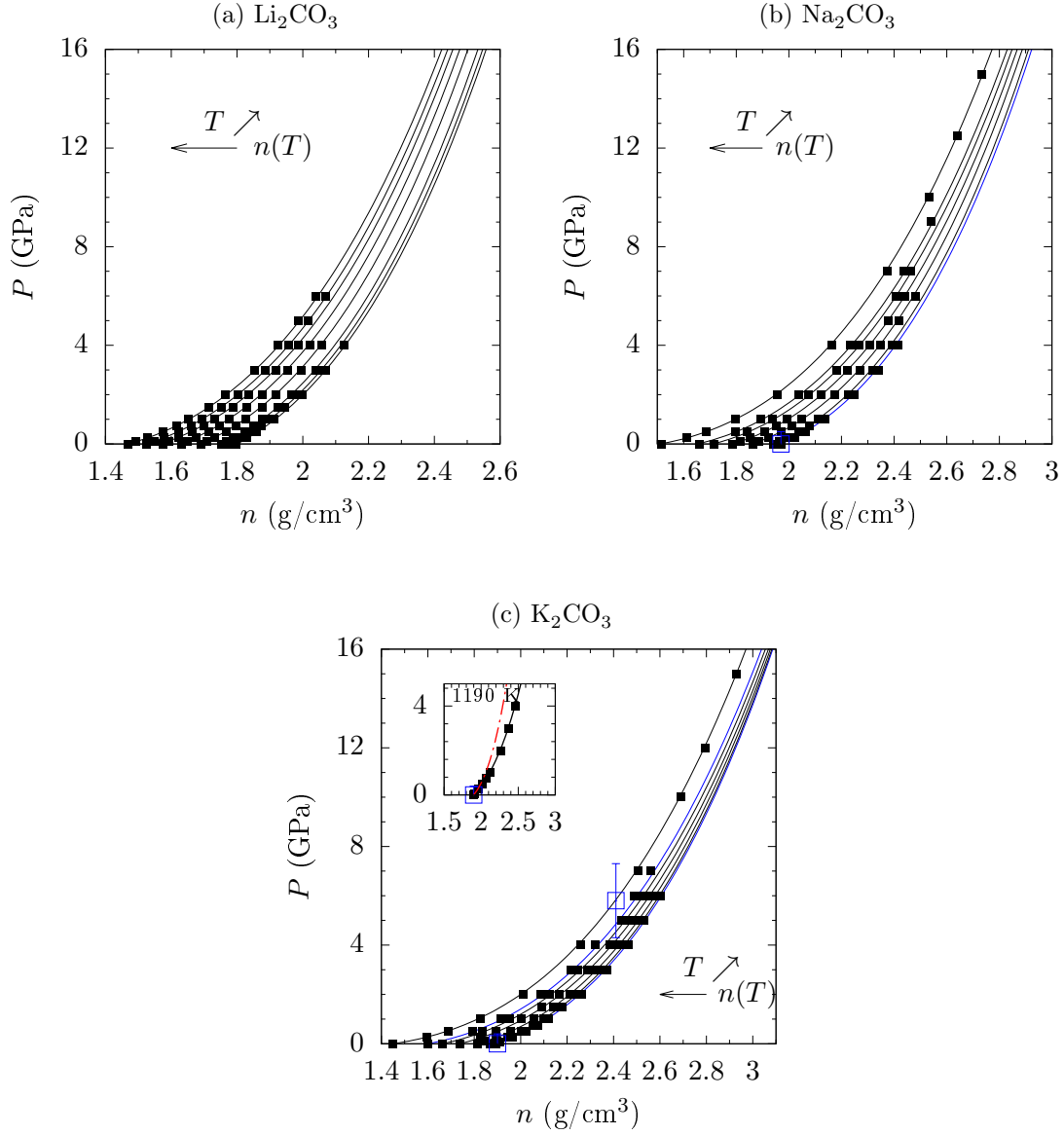


FIG. S2. MD (black) and AIMD (blue) calculated density-pressure points. Compression isotherms (black curves) are interpolated from the MD points by the Birch-Murnaghan equation of state (BMEoS). The temperature of the MD isotherms are {1100 K, 1140 K, 1200 K, 1350 K, 1500 K, 1650 K, 1773 K, 1923 K} for Li_2CO_3 , {1140 K, 1200 K, 1350 K, 1500 K, 1650 K, 1773 K, 2073 K} for Na_2CO_3 and {1190 K, 1240 K, 1350 K, 1500 K, 1650 K, 1773 K, 2073 K} for K_2CO_3 . Blue squares are AIMD points (1140 K for Na_2CO_3 , 1190 K and 1773 K for K_2CO_3). For K_2CO_3 a BMEoS isotherm issued from the experimental thermodynamics data and fusion curve analysis at 1190 K is also plotted in the inset (red curve).^{S4-S6}

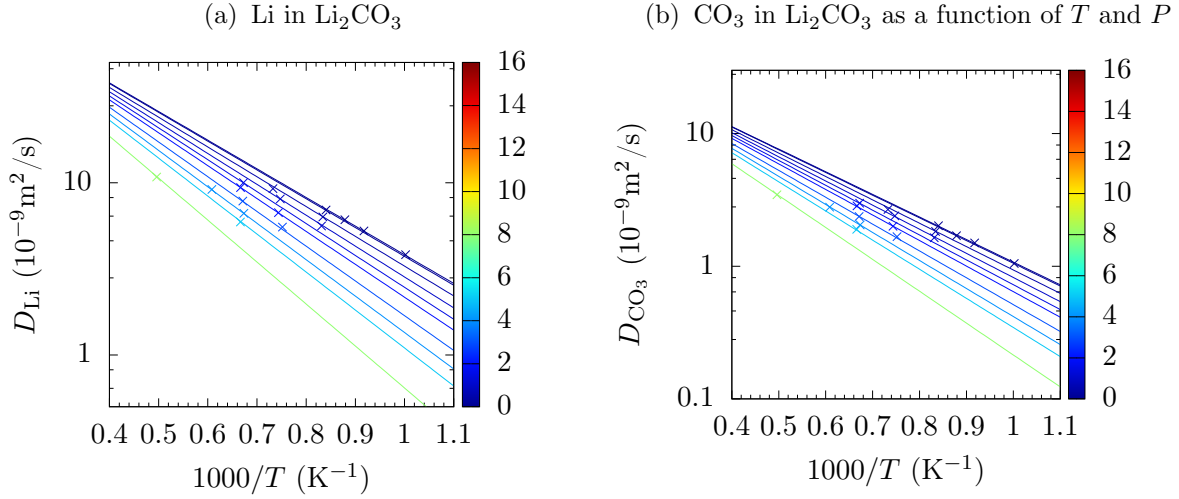


FIG. S3. Diffusion coefficients in Li_2CO_3 calculated by MD (crosses) and isobaric activation laws obtained by fitting all the simulation points. The pressures of the isobars are $\{0.001, 0.05, 0.5, 1, 1.5, 2, 3, 4, 5, 8\}$ in GPa and are referred to with a color code (vertical scale).

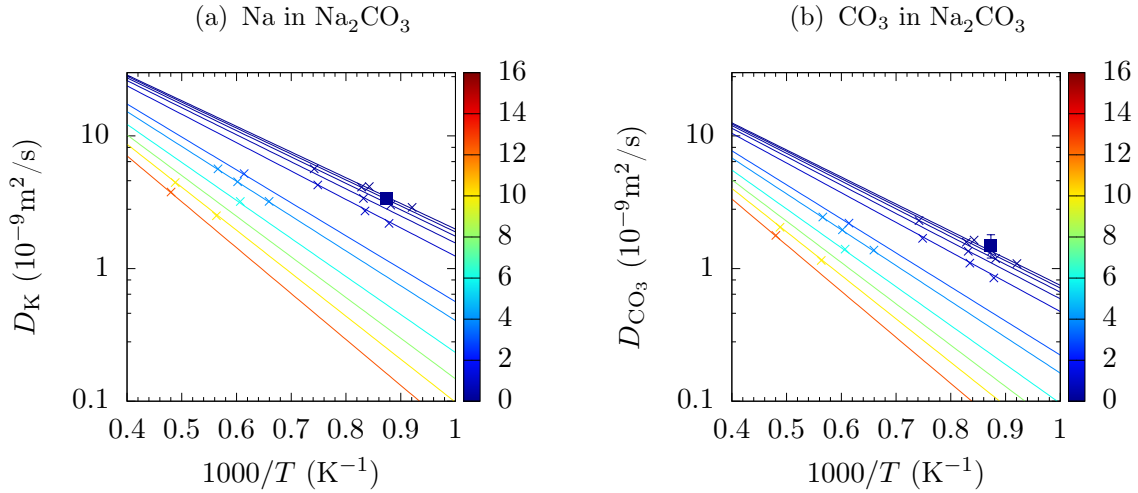


FIG. S4. As Figure S3, but for Na_2CO_3 . The values calculated from the AIMD simulations are represented by plain squares (see Table S1). The pressures of the isobars are $\{0.001, 0.1, 0.25, 0.5, 1, 3, 4, 6, 8, 10, 12.5\}$ in GPa and are referred to with a color code (vertical scale).

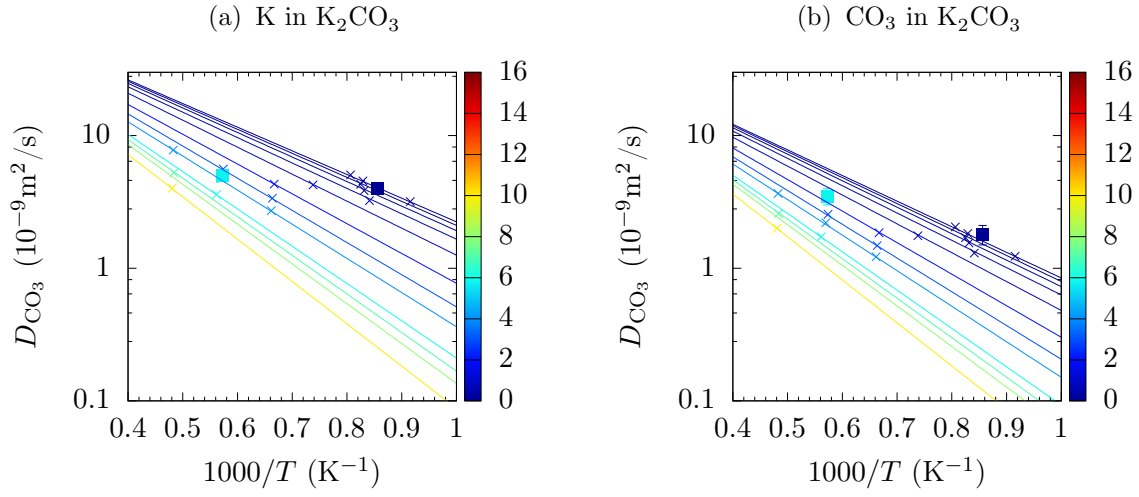


FIG. S5. As Figure S3, but for K_2CO_3 . The values calculated from the AIMD simulations are represented by plain squares (see Table S1). The pressures of the isobars are $\{0.001, 0.25, 0.5, 1, 2, 3, 4, 6, 8, 10\}$ in GPa and are referred to with a color code (vertical scale).

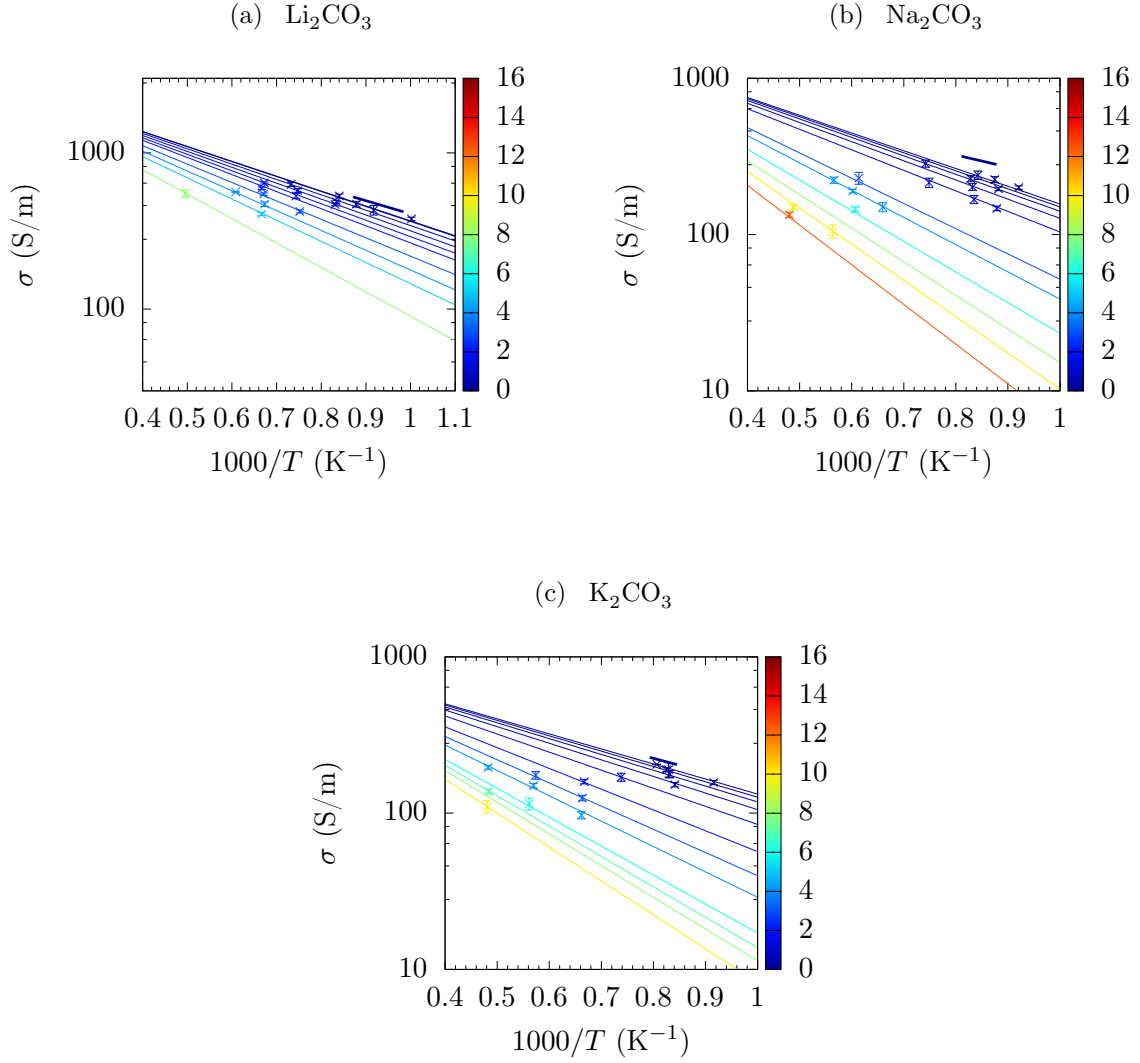


FIG. S6. Electrical conductivity from MD (crosses) and isobaric activation laws (plain lines). The pressures (in GPa) of the isobars are $\{0.001, 0.05, 0.5, 1, 1.5, 2, 3, 4, 5, 8\}$ for Li_2CO_3 , $\{0.001, 0.1, 0.25, 0.5, 1, 3, 4, 6, 8, 10, 12.5\}$ for Na_2CO_3 and $\{0.001, 0.25, 0.5, 1, 2, 3, 4, 6, 8, 10\}$ for K_2CO_3 and are referred to with a color code (vertical scale). Bold segments are experimental values of Kojima^{S7} at $P = 0$.

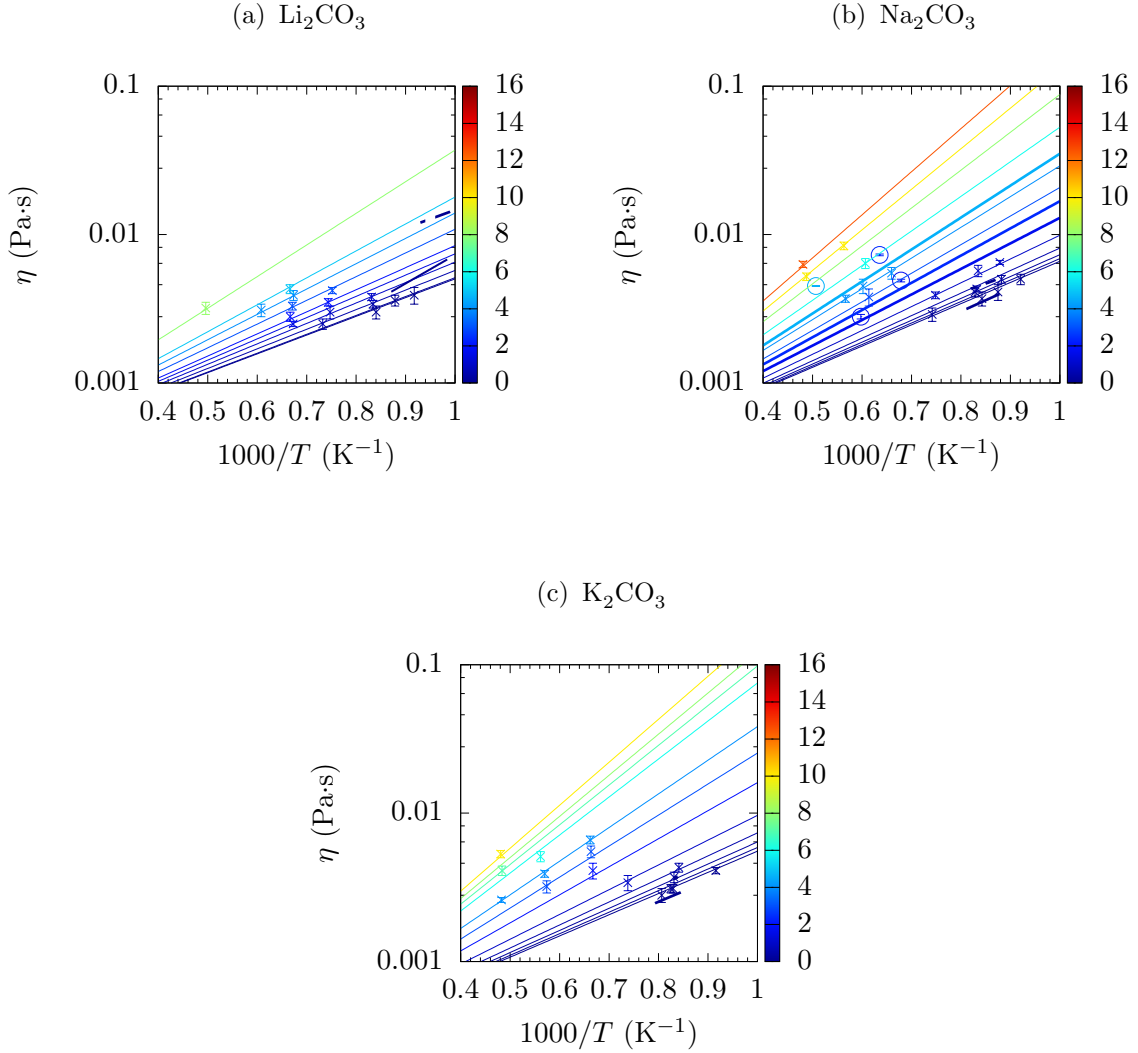


FIG. S7. Viscosity from MD (crosses) and isobaric activation laws obtained for each composition by interpolation of all simulation points. The pressures (in GPa) of the isobars are $\{0.001, 0.05, 0.5, 1, 1.5, 2, 3, 4, 5, 8\}$ for Li_2CO_3 , $\{0.001, 0.1, 0.25, 0.5, 1, 3, 4, 6, 8, 10, 12.5\}$ for Na_2CO_3 and $\{0.001, 0.25, 0.5, 1, 2, 3, 4, 6, 8, 10\}$ for K_2CO_3 and are referred to with a color code (vertical scale). Bold segments are experimental data, those from Janz^{S8} and Sato^{S9} are almost indistinguishable and are thus plotted together as plain lines, whereas the data of Di Genova *et al.*^{S10} are plotted as dotted line. For Na_2CO_3 the high pressure data recently reported by Stagno *et al.*^{S11} are plotted as circles, the corresponding isobars (1.7, 2.4 and 4.6 GPa) obtained from the present MD study are reported for comparison (bold blue lines).

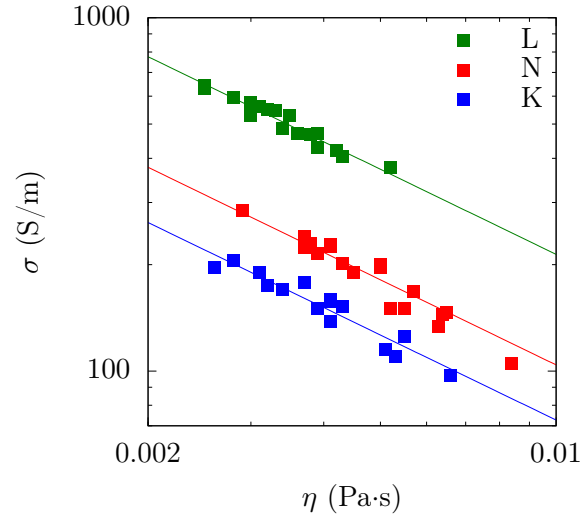


FIG. S8. Electrical conductivity as a function of viscosity. The squares are the MD data and the lines are empirical fits of the MD data by equation $\sigma = A/\eta^{0.8}$ (where σ is in S/m and η in Pa·s) with $A = 5.375$, 2.615 and 1.825 for Li_2CO_3 (L), Na_2CO_3 (N) and K_2CO_3 (K), respectively.

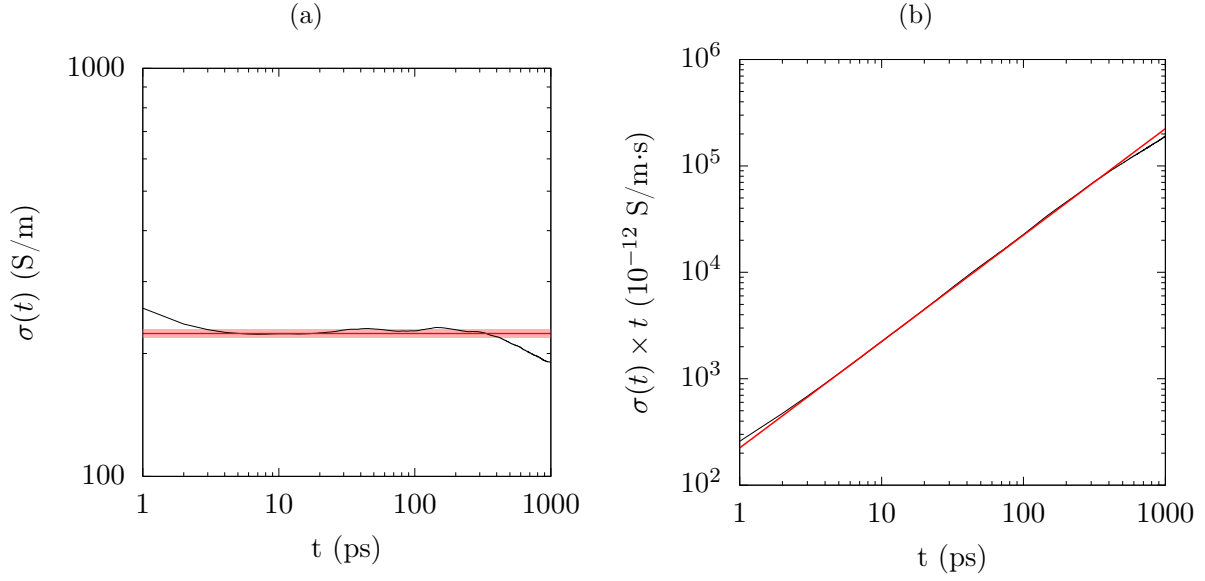


FIG. S9. Example of the method used to estimate the electrical conductivity from the MD simulations. (a) For the conductivity to be calculated the running average $\sigma(t) = \frac{e^2}{k_B T V} \cdot \frac{1}{6t} \left\langle \left| \sum_i z_i (\mathbf{r}_i(t) - \mathbf{r}_i(0)) \right|^2 \right\rangle$ has to reach a plateau (black line). (b) Equivalently convergence is attained when $\sigma(t) \times t$ is linear. In red we plot (a) the calculated conductivity, σ , or (b) $\sigma \times t$, bracketed within uncertainty (red shaded area).

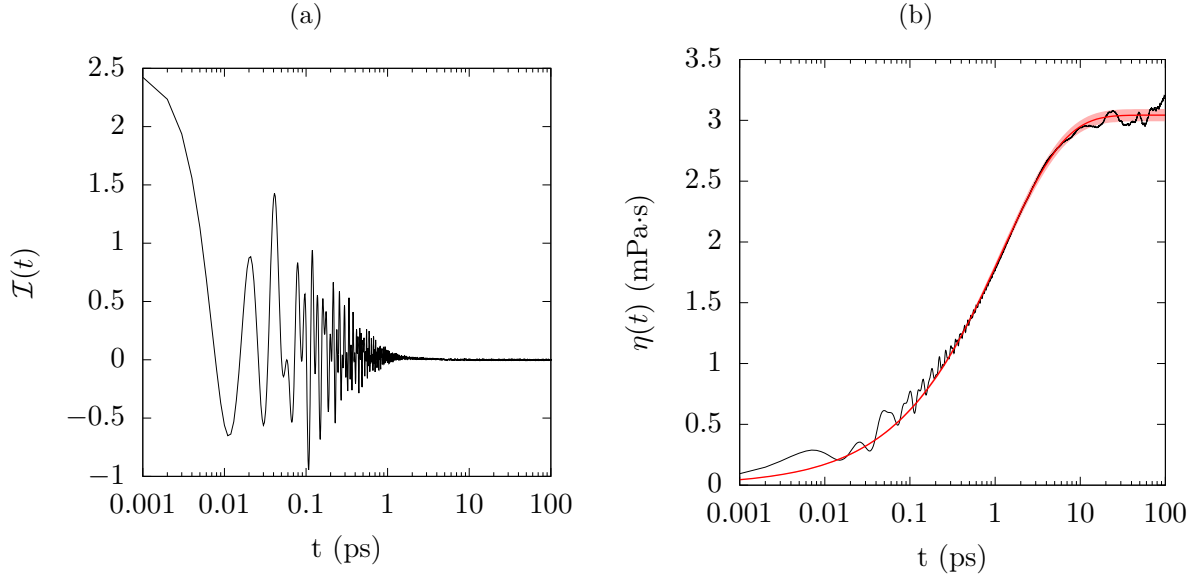


FIG. S10. Example of the method used to estimate the viscosity from the MD simulations. (a) For the viscosity to be calculated the running average $\mathcal{I}(t) = \frac{V}{RT} \langle \Pi_{\alpha\beta}(t) \cdot \Pi_{\alpha\beta}(0) \rangle$, where $\Pi_{\alpha\beta}$ stand for the off-diagonal stress tensor components, has to converge to zero (see equation (12) of main text). (b) To calculate the viscosity, $\eta(t) = \int_0^t dt' \mathcal{I}(t')$ is fitted by a stretched exponential: $\eta_\infty \left(1 - e^{-(t/\tau)^\beta} \right)$ (red), where η_∞ is the viscosity calculated for the considered MD run (i.e. $\eta = \eta_\infty$), τ is a relaxation time and $\beta \in]0; 1]$ is a stretching factor, typically $\beta \in]0.5; 0.65]$.

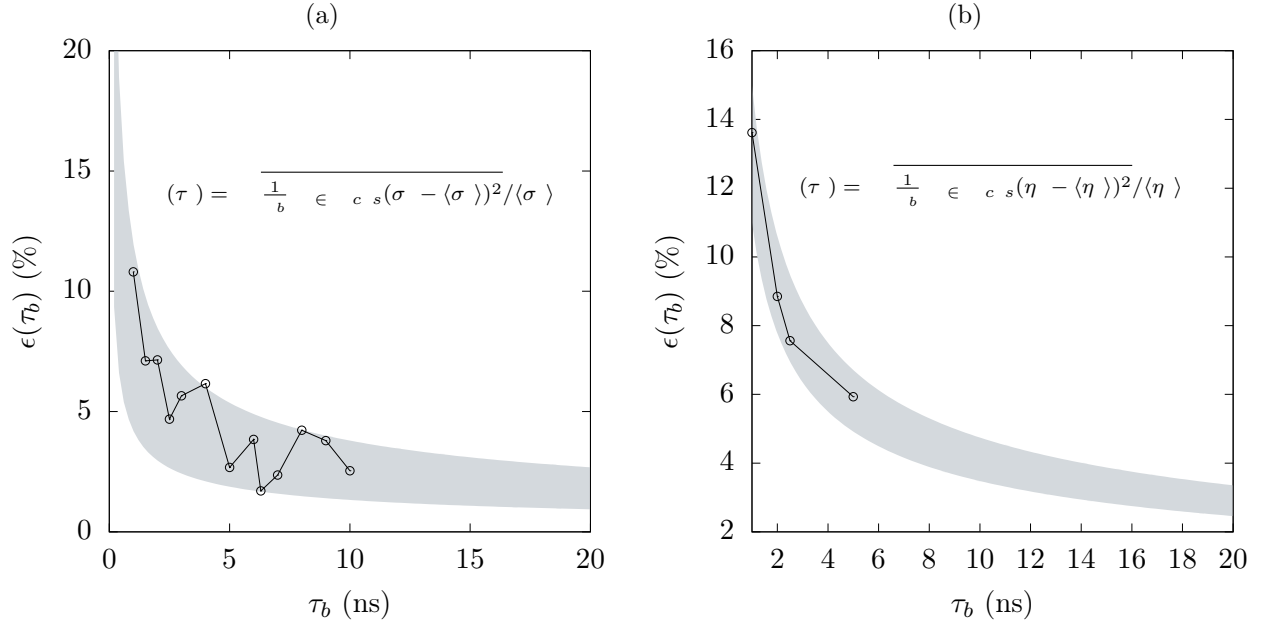


FIG. S11. Estimation of the standard deviation associated to the calculation of the conductivity and of the viscosity as correlation functions (equation (11) and (12) of main text), using a block averaging method. For blocks of different length τ_b , we calculate (a) $\sigma(t) = \frac{e^2}{k_B T V} \cdot \frac{1}{6t} \left\langle \left| \sum_i z_i (\mathbf{r}_i(t) - \mathbf{r}_i(0)) \right|^2 \right\rangle$ or (b) $\eta(t) = \int_0^t dt' \mathcal{I}(t')$, where t is a time at which convergence is attained (see Figure S9 and S10). We arbitrarily chose $t = 20$ ps. Standard deviation as a function of block length, $\epsilon(\tau_b)$, decreases as $1/\tau_b$, as represented by the gray shade. For a typical run length (10 – 30 ns), $\epsilon(\tau_b)$ is below 5 % for the conductivity and for the viscosity. This example is based on a 20 ns long simulation of the Li_2CO_3 melt at 1100 K and 1 bar.

	T	$\langle T \rangle$	n	$\langle P \rangle$	σ	η	D_{Li}	D_{CO_3}
	(K)	(K)	(g/cm ³)	(kbar)	(S/m)	(mPa·s)	(10 ⁻⁹ m ² /s)	(10 ⁻⁹ m ² /s)
Li₂CO₃								
	1000	998	1.84	0	378 ± 10	5.2 ± 0.5	3.82	1.05
	1100	1090	1.80	0	430 ± 30	3.9 ± 0.5	5.25	1.50
	1140	1138	1.78	0	470 ± 20	3.6 ± 0.3	6.10	1.70
	1200	1190	1.77	0.7	530 ± 15	3.0 ± 0.3	6.95	2.02
	1200	1199	1.82	5	487 ± 10	3.4 ± 0.2	6.33	1.83
	1350	1365	1.77	6	630 ± 20	2.5 ± 0.2	9.24	2.68
	1200	1203	1.88	10	467 ± 10	3.8 ± 0.2	5.61	1.64
	1350	1338	1.83	10	574 ± 15	3.0 ± 0.3	8.06	2.40
	1500	1487	1.83	15	642 ± 10	2.5 ± 0.1	10.01	2.99
	1350	1345	1.92	20	530 ± 20	3.5 ± 0.2	6.70	2.00
	1500	1500	1.88	20	593 ± 10	2.8 ± 0.2	9.37	2.85
	1350	1330	1.99	29	422 ± 10	4.2 ± 0.2	5.53	1.67
	1500	1490	1.95	30	545 ± 10	3.3 ± 0.2	7.83	2.37
	1500	1485	2.02	39	470 ± 15	3.9 ± 0.3	6.65	2.05
	1650	1644	1.99	40	562 ± 5	3.1 ± 0.3	9.14	2.79
	1500	1501	2.08	50	406 ± 10	4.3 ± 0.3	5.92	1.90
	2000	2016	2.12	81	550 ± 30	3.2 ± 0.3	10.80	3.46

TABLE S3. Thermodynamic averages and transport coefficients issued from all MD simulations of **Li₂CO₃**.

	T	$\langle T \rangle$	n	$\langle P \rangle$	σ	η	D_{Na}	D_{CO_3}
	(K)	(K)	(g/cm ³)	(kbar)	(S/m)	(mPa-s)	(10 ⁻⁹ m ² /s)	(10 ⁻⁹ m ² /s)
Na₂CO₃								
	1100	1086	2.00	0	200 ± 5	5.0 ± 0.4	2.89	1.09
	1140	1143	1.97	0	225 ± 5	4.1 ± 0.5	3.48	1.36
AIMD	1140	1145	1.97	0 ± 5	/	/	3.4±0.3	1.5 ± 0.3
	1200	1187	1.94	0	242 ± 15	3.7 ± 0.5	4.15	1.62
	2073	2055	1.50	0	465 ± 10	0.86 ± 0.03	21.42	9.78
	1200	1207	1.93	1.2	228 ± 10	4.1 ± 0.3	4.11	1.58
	1140	1134	2.02	2.3	196 ± 5	5.0 ± 0.3	3.01	1.19
	1350	1348	1.92	2.5	285 ± 15	2.9 ± 0.1	5.65	2.30
	1200	1202	2.04	5.0	202 ± 10	4.3 ± 0.2	3.38	1.35
	1140	1138	2.14	9.9	147 ± 5	6.5 ± 0.2	2.19	0.85
	1200	1198	2.11	9.9	168 ± 10	5.7 ± 0.5	2.72	1.10
	1350	1336	2.05	9.7	215 ± 15	3.9 ± 0.2	4.27	1.69
	1650	1629	2.18	29	230±20	3.8± 0.5	5.20	2.20
	1500	1516	2.31	40	154 ± 10	5.5 ± 0.5	3.21	1.38
	1650	1661	2.27	40	190 ± 5	4.5 ± 0.5	4.51	1.96
	1773	1766	2.23	40	223 ± 10	3.7 ± 0.2	5.65	2.45
	1650	1648	2.41	60	145±5	6.4 ± 0.5	3.20	1.40
	1773	1775	2.59	100	105 ± 10	8.4 ± 0.5	2.50	1.15
	2073	2049	2.53	99	150 ± 5	5.2 ± 0.3	4.45	2.05
	2073	2081	2.64	125	134 ± 5	6.3 ± 0.3	3.78	1.78

TABLE S4. Thermodynamic averages and transport coefficients issued from all MD simulations of **Na₂CO₃**. Diffusion coefficients estimated from the AIMD simulation are also mentioned (AIMD).

	T	$\langle T \rangle$	n	$\langle P \rangle$	σ	η	D_K	D_{CO_3}
	(K)	(K)	(g/cm ³)	(kbar)	(S/m)	(mPa·s)	(10 ⁻⁹ m ² /s)	(10 ⁻⁹ m ² /s)
K₂CO₃								
	1100	1092	1.94	0	157 ± 5	4.1 ± 0.2	3.18	1.23
	1200	1206	1.89	0	190 ± 20	3.1 ± 0.2	4.55	1.83
AIMD	1190	1168	1.90	0 ± 4	/	/	4.0 ± 0.2	1.8 ± 0.3
	1240	1240	1.87	0	205 ± 5	2.8 ± 0.3	5.05	2.03
	1200	1212	1.92	1.2	195 ± 10	3.1 ± 0.2	4.30	1.70
	1190	1203	1.96	2.7	178 ± 10	3.7 ± 0.3	3.85	1.55
	1190	1189	2.02	4.9	152 ± 5	4.3 ± 0.3	3.23	1.30
	1350	1355	2.06	10	170 ± 10	3.4 ± 0.4	4.25	1.76
	2073	2025	1.83	9.4	318 ± 5	1.6 ± 0.1	14.05	6.35
	1500	1499	2.17	20	159 ± 5	4.1 ± 0.5	4.31	1.85
	1500	1507	2.29	30	125 ± 5	5.5 ± 0.5	3.37	1.48
	1773	1742	2.22	29	175 ± 10	3.2 ± 0.3	5.60	2.55
	1500	1511	2.39	40	97 ± 5	6.6 ± 0.4	2.72	1.22
	1773	1755	2.32	40	150 ± 5	3.9 ± 0.2	4.75	2.20
	2073	2072	2.26	40	196 ± 5	2.6 ± 0.1	7.78	3.66
	1773	1781	2.49	60	115 ± 10	5.1 ± 0.4	3.60	1.73
AIMD	1773	1748	2.41	58 ± 15	/	/	5.0 ± 0.5	3.5 ± 0.5
	2073	2068	2.51	70	138 ± 5	4.1 ± 0.3	5.25	2.58
	2073	2080	2.69	100	110 ± 10	5.3 ± 0.3	4.00	2.00

TABLE S5. Thermodynamic averages and transport coefficients issued from all MD simulations of **K₂CO₃**. Diffusion coefficients estimated from the AIMD simulations are also mentioned (AIMD).

	T	$\langle T \rangle$	n	$\langle P \rangle$	σ	η	D_{X_1}	D_{X_2}	D_{CO_3}
	(K)	(K)	(g/cm ³)	(kbar)	(S/m)	(mPa·s)	(10 ⁻⁹ m ² /s)	(10 ⁻⁹ m ² /s)	(10 ⁻⁹ m ² /s)
Li₂CO₃-Na₂CO₃									
0.70: 0.30	1100	1102	1.87	0	330 ± 15	3.9 ± 0.3	4.55	3.68	1.39
	1173	1169	1.84	0	350 ± 10	3.4 ± 0.5	5.55	4.48	1.78
0.53: 0.47 (LNe)	800	793	2.06	0	84 ± 5	18 ± 2	0.81	0.62	0.22
	1000	979	1.95	0	208 ± 10	7.0 ± 1	2.59	2.15	0.78
	1100	1089	1.90	0	265 ± 10	4.4 ± 0.2	3.98	3.41	1.28
0.30: 0.70	1100	1088	1.95	0	9	4.6 ± 0.2	3.54	3.14	1.18
Li₂CO₃-K₂CO₃									
0.70: 0.30	1100	1102	1.84	0	326 ± 10	4.0 ± 0.3	4.54	3.69	1.40
	1173	1170	1.83	0	275 ± 15	3.1 ± 0.3	4.95	3.95	1.78
0.62: 0.38 (LKe)	900	894	1.98	0	105 ± 5	10.5 ± 0.5	1.44	1.11	0.45
	1100	1096	1.88	0	200 ± 10	3.9 ± 0.3	3.65	3.05	1.31
0.50: 0.50	1100	1082	1.89	0	186 ± 5	4.2 ± 0.2	3.23	2.93	1.25
0.43: 0.57 (LKe2)	900	902	1.99	0	88 ± 5	10.5 ± 1	1.22	1.12	0.42
	1100	1092	1.91	0	170 ± 10	3.9 ± 0.3	2.99	2.90	1.20
0.30: 0.70	1100	1093	1.92	0	157 ± 5	4.0 ± 0.2	2.85	3.05	1.24
Na₂CO₃-K₂CO₃									
0.58: 0.42	1000	995	2.02	0	124 ± 10	7.0 ± 0.5	1.89	1.81	0.70
	1073	1070	1.99	0	148 ± 5	5.0 ± 0.3	2.62	2.59	1.00
0.50: 0.50 (NK)	1040	1038	2.00	0	136 ± 5	6.4 ± 0.5	2.27	2.27	0.86
	1200	1185	1.91	0	195 ± 15	3.1 ± 0.4	4.00	4.08	1.60

TABLE S6. Thermodynamic averages and transport coefficients issued from all MD simulations of binary mixtures **Li₂CO₃-Na₂CO₃**, **Li₂CO₃-K₂CO₃** and **Na₂CO₃-K₂CO₃**. The notation X_1 (= Li or Na) and X_2 (= Na or K) are attributed in the same order as appearing in the composition name (first column).

	T	$\langle T \rangle$	n	$\langle P \rangle$	σ	η	D_{Li}	D_{Na}	D_{K}	D_{CO_3}
	(K)	(K)	(g/cm ³)	(kbar)	(S/m)	(mPa-s)	(10 ⁻⁹ m ² /s)			
Li ₂ CO ₃ -Na ₂ CO ₃ -K ₂ CO ₃										
0.435: 0.315: 25 (LNKe)	750	743	2.10	0	40 ± 5	35 ± 5	0.37	0.30	0.26	0.10
	900	896	2.02	0	107 ± 10	10.7 ± 0.3	1.38	1.20	1.05	0.44
	1050	1048	1.94	0	188 ± 10	4.9 ± 0.3	2.88	2.67	2.38	1.02
0.33: 0.33: 0.33 (LNK)	900	893	2.03	0	90 ± 10	13.7 ± 1	1.21	1.13	1.02	0.40
	1073	1072	1.93	0	176 ± 10	4.5 ± 0.3	3.01	2.90	2.68	1.13

TABLE S7. Thermodynamic averages and transport coefficients issued from all MD simulations of ternary mixtures **Li₂CO₃-Na₂CO₃-K₂CO₃**.

	T	$\langle T \rangle$	n	$\langle P \rangle$	γ	γ_{Exp}
	(K)	(K)	(g/cm ³)	(kbar)	(mN/m)	(mN/m)
Li ₂ CO ₃	1100	1089	1.80	-0.4	263 ± 5	240 ^{S7}
	1140	1138	1.78	-0.2	259 ± 3	239 ^{S7}
	1200	1195		-0.4	256 ± 5	236 ^{S7}
Na ₂ CO ₃	1140	1137	1.97	-0.3	224 ± 5	211 ^{S7}
	1200	1203	1.94	-0.2	219 ± 4	208 ^{S7}
K ₂ CO ₃	1200	1168	1.89	-0.3	178 ± 4	167 ^{S7}
	1240	1225	1.87	-0.2	171 ± 4	165 ^{S7}

TABLE S8. Surface tension from MD. For comparison values from the experimental literature are also reported (γ_{Exp}).

	T (K)	$\langle T \rangle$ (K)	n (g/cm ³)	$\langle P \rangle$ (kbar)	γ (mN/m)	γ_{Exp} (mN/m)
<hr/>						
Li ₂ CO ₃ -Na ₂ CO ₃						
0.70: 0.30	1173	1166	1.84	-0.4	246 ± 3	228 ^{S7}
0.53:0.47 (LNe)	900	911	2.00	-0.3	269 ± 5	249 ^{S7}
	1100	1094	1.90	-0.2	247 ± 3	231 ^{S7}
<hr/>						
Li ₂ CO ₃ -K ₂ CO ₃						
0.70: 0.30	1173	1178	1.83	-0.2	211 ± 3	195 ^{S7}
0.62: 0.38 (LKe)	900	882	1.98	-0.2	250 ± 3	207 ^{S7}
	1100	1093	1.88	-0.2	223 ± 3	193 ^{S7}
<hr/>						
Na ₂ CO ₃ -K ₂ CO ₃						
0.50: 0.50	1040	1036	2.00	-0.2	212 ± 6	189 ^{S7}
	1100	1093	1.97	-0.3	204 ± 3	185 ^{S7}
	1200	1197	1.91	-0.2	191 ± 5	179 ^{S8}
<hr/>						
Li ₂ CO ₃ -Na ₂ CO ₃ -K ₂ CO ₃						
0.435: 0.315: 25 (LNKe)	750	749	2.10	-0.2	269 ± 5	223 ^{S7}
	900	897	2.02	-0.2	246 ± 2	213 ^{S7}
	1200	1200	1.88	-0.2	209 ± 3	194 ^{S7}
0.33: 0.33: 0.33 (LNK)	900	905	2.03	-0.2	239 ± 3	207 ^{S7}
	1100	1094	1.93	-0.2	220 ± 4	194 ^{S7}
<hr/>						

TABLE S9. Surface tension from MD for binary and ternary mixtures. For comparison values from the experimental literature are also reported (γ_{Exp}).

CP2K INPUT FILE EXAMPLE

```
# CP2K input file example for Supplementary Material for
# "Atomistic simulations of molten carbonates:
# thermodynamic and transport properties of the Li2CO3 - Na2CO3 - K2CO3 system"
@SET RESTART 1
@SET LIBDIR /scratch/desmaele/cp2k/files
@SET SYSTEM K2CO3
& FORCE_EVAL
  METHOD QuickStep
  STRESS_TENSOR DIAGONAL_ANALYTICAL
& DFT
  BASIS_SET_FILE_NAME ${LIBDIR}/BASIS_MOLOPT
  POTENTIAL_FILE_NAME ${LIBDIR}/GTH_POTENTIALS
& MGRID
  CUTOFF 700
  NGRIDS 6
  REL_CUTOFF 40
& END MGRID
& QS
  EPS_DEFAULT 1.0E-12
  MAP_CONSISTENT TRUE
  EXTRAPOLATION ASPC
  EXTRAPOLATION_ORDER 3
& END QS
& SCF
  MAX_SCF 20
  SCF_GUESS RESTART
  EPS_SCF 3.0E-7
& OUTER_SCF
  EPS_SCF 3.0E-7
  MAX_SCF 1000
```

```

& END OUTER_SCF
& OT ON
  PRECONDITIONER FULL_SINGLE_INVERSE
  MINIMIZER DIIS
  N_DIIS 6
& END OT
& PRINT
  & RESTART_HISTORY
  BACKUP_COPIES 0
  & END RESTART_HISTORY
& END PRINT
& END SCF
& XC
  & XC_FUNCTIONAL BLYP
  & END XC_FUNCTIONAL
  & vdW_POTENTIAL
  DISPERSION_FUNCTIONAL PAIR_POTENTIAL
  & PAIR_POTENTIAL
  PARAMETER_FILE_NAME ${LIBDIR}/dftd3.dat
  TYPE DFTD3
  REFERENCE_FUNCTIONAL BLYP
  R_CUTOFF 30.0
  & END PAIR_POTENTIAL
& END vdW_POTENTIAL
& XC_GRID
  XC_DERIV SPLINE3
& END XC_GRID
& END XC
& END DFT
& SUBSYS
& CELL
  ABC [angstrom] 16.0244 16.0244 16.0244

```

```

& END CELL
& TOPOLOGY
  COORD_FILE_FORMAT xyz
  COORD_FILE_NAME ./k2co3.xyz
  CONNECTIVITY OFF
& END TOPOLOGY
& KIND C
  BASIS_SET DZVP-MOLOPT-SR-GTH-q4
  POTENTIAL GTH-BLYP-q4
& END KIND
& KIND O
  BASIS_SET DZVP-MOLOPT-SR-GTH-q6
  POTENTIAL GTH-BLYP-q6
& END KIND
& KIND K
  BASIS_SET DZVP-MOLOPT-SR-GTH-q9
  POTENTIAL GTH-BLYP-q9
& END KIND
& END SUBSYS
& END FORCE_EVAL
& GLOBAL
  PROJECT ${SYSTEM}
  RUN_TYPE MD
  PRINT_LEVEL LOW
  WALLTIME 86370
& END GLOBAL
& MOTION
  & MD
    ENSEMBLE NVT
    STEPS 100000
    TIMESTEP 0.5
    TEMPERATURE 1190

```

```

& THERMOSTAT
  TYPE CSV
  & CSV
    TIMECON [fs] 1000
  & END CSV
  & NOSE
    LENGTH 4
    YOSHIDA 9
    TIMECON [fs] 500.0
    MULTIPLE.TIME.STEPS 2
  & END NOSE
& END THERMOSTAT
& END MD
& PRINT
  & STRESS  ON
    FILENAME =${SYSTEM}.stress
  & EACH
    MD 1
  & END EACH
& END STRESS
& TRAJECTORY  ON
  FILENAME =${SYSTEM}.xyz
  & EACH
    MD 1
  & END EACH
& END TRAJECTORY
& VELOCITIES  ON
  FILENAME =${SYSTEM}.vel
  & EACH
    MD 1
  & END EACH
& END VELOCITIES

```

```

& FORCES ON
  FILENAME =${SYSTEM}.force
  & EACH
    MD 1
  & END EACH
& END FORCES
& RESTART
  FILENAME =${SYSTEM}.restart
  & EACH
    MD 1
  & END EACH
& END RESTART
& END PRINT
& END MOTION
@if ${RESTART} == 1
& EXT_RESTART
  RESTART_FILE_NAME ${SYSTEM}.restart
  RESTART_COUNTERS T
  RESTART_AVERAGES T
  RESTART_POS T
  RESTART_VEL T
  RESTART_THERMOSTAT T
& END EXT_RESTART
@endif

```

REFERENCES

- [S1]Y. Idemoto, J. W. Richardson, N. Koura, S. Kohara, and C.-K. Loong, *J. Phys. Chem. Solids* **59** (1998).
- [S2]A. Arakcheeva, L. Bindi, P. Pattison, N. Meisser, G. Chapuis, and I. Pekov, *Am. Mineral.* **95** (2010).
- [S3]B. M. Gatehouse and D. J. Lloyd, *J. Chem. Soc., Dalton Trans* (1973).
- [S4]Q. Liu and R. Lange, *Contrib. Mineral. Petrol.* **146** (2003).
- [S5]M. C. O’Leary, R. A. Lange, and Y. Ai, *Contrib. Mineral. Petrol.* **170** (2015).
- [S6]M. Wang, Q. Liu, T. Inoue, B. Li, S. Pottish, J. Wood, C. Yang, and R. Tao, *J. Mineral. Petrol. Sci.* **111** (2016).
- [S7]T. Kojima, *Physical and Chemical Properties of Molten Carbonates*, Ph.D. thesis, Kobe University (2009).
- [S8]G. J. Janz, *J. Phys. Chem. Ref. Data* **Suppl. 2** (1988).
- [S9]Y. e. a. Sato, *Netsu Bussei* **13** (1999).
- [S10]D. Di Genova, C. Cimarelli, K.-U. Hess, and D. B. Dingwell, *Am. Mineral.* **101** (2016).
- [S11]V. Stagno, V. Stopponi, Y. Kono, C. E. Manning, and T. Irifune, *Chem. Geol.* (*in press*).